HHS Public Access

Author manuscript

Nat Cardiovasc Res. Author manuscript; available in PMC 2023 May 11.

Published in final edited form as:

Nat Cardiovasc Res. 2022 November ; 1(11): 1084–1100. doi:10.1038/s44161-022-00162-1.

Generation and Comparative Analysis of an *Itga8-CreER^{T2}* Mouse with Preferential Activity in Vascular Smooth Muscle Cells

Ganesh Warthi[1], **Jessica L. Faulkner**[2], **Jaser Doja**[1], **Amr R. Ghanam**[1], **Pan Gao**[1], **Allison C. Yang**[1], **Orazio J. Slivano**[1], **Candee T. Barris**[1], **Taylor C. Kress**[1], **Scott D. Zawieja**[3], **Susan H. Griffin**[1], **Xiaoling Xie**[4], **Alan Ashworth**[5], **Christine K. Christie**[6], **William B. Bryant**[1], **Ajay Kumar**[1], **Michael J. Davis**[3], **Xiaochun Long**[1], **Lin Gan**[4], **Eric J. Belin de Chantemèle**[1], **Qing Lyu**[1,7,8,*], **Joseph M. Miano**[1,*]

[1]Vascular Biology Center, Medical College of Georgia at Augusta University, Augusta, Georgia 30912

[2]Department of Physiology, Medical College of Georgia at Augusta University, Augusta, Georgia 30912

[3]Medical Pharmacology and Physiology, University of Missouri School of Medicine, Columbia, MO 65212

[4]Department of Neuroscience and Regenerative Medicine, Medical College of Georgia at Augusta University, Augusta, Georgia 30912

[*]Corresponding Authors: Joseph M. Miano, PhD, Vascular Biology Center, Medical College of Georgia at Augusta University, 1460 Laney Walker Boulevard, Augusta, Georgia 30912, jmiano@augusta.edu, 706-446-0166 (Phone), 706-721-9799 (FAX); Qing Lyu, PhD, Biomedical and Health Institute, Chongqing Institute of Green and Intelligence Technology, Chinese Academy of Sciences, Chongqing 400714, China, lvqing@cigit.ac.cn.

Author Contributions

GDW helped develop the figures and performed Western blotting studies in Extended Data Figs. 2e, 6d, and 8a-8b and Figs. 2b and 3g-3h; bulk RNA-seq studies in Fig. 2e and Supplementary Table 2; Figs. 3a-3b; assistance with the blood pressure studies of Figs. 4 and 5; and performing the myography studies of Fig. 6. JLF performed and/or analyzed vascular function and blood pressure data of Figs. 4, 5 and 6a-6c and wrote the methods section related to these experiments. JD performed the studies in Fig. 3c, 3d, and Extended Data Fig. 10 and conducted tamoxifen injections for studies of blood pressure and myography measurements. ARG provided foundational work and helped generate Supplementary Fig. 1. PG assisted with Western blotting studies of Extended Data Fig. 2a-b. ACY generated the data for Supplementary Fig. 2. OJS performed all histology, immunostaining, confocal immunofluorescence and bright-field microscopy and generated all of the images, save lymphatic vessels. MJD and SDZ planned and performed experiments in Figs. 3e and 3f and Extended Data Fig. 6 and 7; they also contributed to the writing and editing of the methods and results. CKC, ACY, and SHG did all breeding and genotyping of mice. CKC provided images to Extended Data Figs. 8c and 9a. CTB helped perform the telemetry experiments of Figs. 4 and 5. TCK isolated aortas and helped run myography experiments in Fig. 6. WBB prepared and analyzed the Sanger sequencing of the *Cre* in *Myh11-CreER^{T2}* of Supplementary Fig. 3 and the long read sequence mapping of *Myh11-CreER^{T2}* in Fig. 2c and 2d. AA helped with the interpretation of *Myh11-CreER^{T2}* mapping and the design of Fig. 2d. AK contributed to Western blotting studies of Fig. 2b. XL contributed to data in Fig. 2a and provided intellectual input on study design and interpretation. LG and XX designed and generated the *Itga8-CreER^{T2}* mouse and developed Extended Data Fig. 1 (top). EBC helped with the acquisition and interpretation of the blood pressure and vascular reactivity data. QL performed studies in Extended Data Figs. 2, 3, 9b-9g, Supplementary Fig. 4b, 4d, and Fig. 7; he also provided intellectual input throughout the study and finalized the figures. JMM conceived and supervised the entire project, analyzed all data, developed Extended Data Fig. 1 (bottom) and Supplemental Fig. 5, assembled original Western blots in Extended Data Fig. 4a-c, 5, and Supplemental Fig. 6 and outlined, wrote, and edited the manuscript.

Competing Interests

A.A. is a co-founder of Tango Therapeutics, Azkarra Therapeutics, Ovibio Corporation and Kytarro; a member of the board of Cytomx and Cambridge Science Corporation; a member of the scientific advisory board of Genentech, GLAdiator, Circle, Bluestar, Earli, Ambagon, Phoenix Molecular Designs and Trial Library; a consultant for SPARC, ProLynx, and GSK; receives grant or research support from SPARC and AstraZeneca, and holds patents on the use of PARP inhibitors held jointly with AstraZeneca from which he has benefited financially (and may do so in the future). The patents are unrelated to any aspect of the current study. All other authors declare no competing interests.

[5]Helen Diller Family Comprehensive Cancer Center, University of California San Francisco, San Francisco, CA, 94158

[6]Cardiovascular Research Institute, University of Rochester School of Medicine and Dentistry, Rochester, New York 14642

[7]Biomedical and Health Institute, Chongqing Institute of Green and Intelligence Technology, Chongqing, China 400714

[8]Chongqing General Hospital, Chongqing, China 401147

Abstract

All current smooth muscle cell (SMC) *Cre* mice similarly recombine floxed alleles in vascular and visceral SMCs. Here, we present an *Itga8-CreER^{T2}* knock-in mouse and compare its activity with a *Myh11-CreER^{T2}* mouse. Both *Cre* drivers demonstrate equivalent recombination in vascular SMCs. However, *Myh11-CreER^{T2}* mice, but not *Itga8-CreER^{T2}* mice, display high activity in visceral SMC-containing tissues such as intestine, show early tamoxifen-independent activity, and produce high levels of CreER^{T2} protein. Whereas *Myh11-CreER^{T2}*-mediated knockout of serum response factor (*Srf*) causes a lethal intestinal phenotype precluding analysis of the vasculature, loss of *Srf* with *Itga8-CreER^{T2}* (*Srf^{Itga8}*) yields viable mice with no evidence of intestinal pathology. Male and female *Srf^{Itga8}* mice exhibit vascular contractile incompetence, and angiotensin II causes elevated blood pressure in wild type, but not *Srf^{Itga8}*, male mice. These findings establish the *Itga8-CreER^{T2}* mouse as an alternative to existing SMC *Cre* mice for unfettered phenotyping of vascular SMCs following selective gene loss.

Editor summary:

Warthi and colleagues generate an alpha 8 integrin-cre driver that enables gene targeting specifically in vascular smooth muscle cells, and show in a proof-of-principle study that using the Itga8-CreERT2 knock-in mouse for selective ablation of the Srf gene causes vascular defects but not a lethal visceral myopathy observed in a smooth muscle cell-specific Myh11-CreERT2-driven Srf loss, attesting to an increased vascular muscle cell-specificity of the Itga8-CreERT locus.

Keywords

mouse; Cre recombinase; knockout; smooth muscle; serum response factor; integrin alpha 8

Conditional gene disruption requires two components derived from bacteriophage P1: a *C*yclization *re*combination (*Cre*) gene encoding a 343 amino acid (38 kDa) tyrosine site-specific recombinase and 34-base pair *lo*cus of crossing (*x*) over of P1 (*lox*P) sequences having dyad symmetry, flanking (or floxing) the region of DNA to be excised.[1] The first application of the *Cre*/*lox*P system for conditional knockout of a gene utilized an *Lck* promoter-driven *Cre* transgene to inactivate *Polb* in T cells.[2] Soon after, temporal inactivation of a gene was introduced with the fusion of Cre to a tamoxifen-responsive ligand binding domain of the estrogen receptor.[3] These pioneering studies underscore two considerations in the design of conditional knockout experiments: judicious placement of *lox*P sites around a sequence to be excised and selection of a well-characterized, cell-

restricted *Cre* driver. The spatial control of *Cre* expression is of crucial importance for gene disruption in smooth muscle cells (SMCs) which enfold and support blood and lymphatic vessels, the airways of the respiratory system, and all hollow organs of the abdominal cavity.

SMCs have distinct embryological origins[4, 5] and contractile properties,[6, 7] but they express a common set of cell-restricted genes that maintain normal SMC homeostasis.[8] Several of these genes have been harnessed for the development of SMC *Cre* driver mice, each of which has advantages and disadvantages.[9] A shared characteristic of all current SMC *Cre* driver mice is the comparable recombination activity in both vascular and visceral SMC lineages.[9] SMC-wide Cre activity can lead to severe, often lethal, visceral myopathies that impede efforts to understand the biology of key genes within vascular SMCs (VSMCs).[10-14] Further, whole-body knockout of some SMC-restricted genes results in embryonic or postnatal death, portending lethality even with an SMC conditional knockout approach.[15-18] Various gene editing strategies will accelerate the development of new floxed alleles for conditional knockout studies in SMCs,[19-22] and many gene products will likely be essential for visceral SMC homeostasis. Thus, a more VSMC-restricted *Cre* driver mouse is urgently needed to avoid the confounding effects of visceral myopathies observed with existing SMC *Cre* strains.

Alpha 8 integrin (*Itga8*) was first cloned from an embryonic chicken cDNA library and the 160 kilodalton protein was shown to interact with the beta 1 integrin subunit.[23] Expression studies demonstrated ITGA8 protein in VSMCs and mesangial cells (an SMC-like cell) of the adult rat kidney.[24, 25] A subtractive hybridization screen in VSMCs reported a partial cDNA to rat *Itga8* that was used to show prominent *Itga8* mRNA in the adult rat aorta.[26] Subsequent work demonstrated the down-regulation of ITGA8 with vascular injury[27] and its role in the maintenance of VSMC differentiation.[28] A more recent study found abundant *Itga8* mRNA in VSMCs, with minimal expression in visceral SMC-containing tissues of mouse, rat, and human origin. This prompted a suggestion that *Itga8* might represent an ideal locus for targeting with an inducible *Cre* to establish a new mouse model for VSMC-restricted knockout studies.[29] Here, the generation and characterization of an *Itga8-CreER^{T2}* mouse are reported. Comparative studies indicate important advantages of the *Itga8-CreER^{T2}* mouse over existing SMC *Cre* drivers for the unambiguous determination of gene function in VSMCs.

Results

Itga8-CreER^{T2} mice expressed normal levels of ITGA8

Compared to most traditional SMC markers, *Itga8* mRNA is preferentially expressed in VSMCs (Supplementary Fig. 1). Accordingly, the first exon of *Itga8* was targeted with a *CreER^{T2}* cassette in embryonic stem cells to establish a new inducible *CreER^{T2}* mouse (Extended Data Fig. 1). Mice homozygous for *Itga8-CreER^{T2}* displayed renal agenesis and postnatal death (Supplementary Fig. 2), a phenotype consistent with a previous *Itga8* loss-of-function study.[30] Because ITGA8 protein expression was not reported in heterozygous knockout mice,[30] it was important to determine whether one functional *Itga8* allele is sufficient for normal levels of ITGA8 protein. Heterozygous *Itga8-CreER^{T2}* aorta showed indistinguishable levels of ITGA8 protein and a slight reduction of *Itga8* mRNA versus

wild type aorta (Extended Data Fig. 2a,b). There was little change in the expression of a 5' overlapping nuclear long noncoding RNA (Supplementary Fig. 1 and Extended Data Fig. 2c,d). Male and female *Itga8-CreER^{T2}* mice exhibited similar levels of ITGA8 and CreER^{T2} protein in the aorta (Extended Data Fig. 2e) and they bred well with no overt signs of pathology. These results demonstrated wild type levels of ITGA8 protein with only one functional *Itga8* allele, thus supporting accurate phenotyping of *Itga8-CreER^{T2}*-mediated gene knockouts without the confounding effects of attenuated ITGA8 protein.

Neither *CreER^{T2}* showed recombination activity in myeloid cells

Over 340 floxed genes have been targeted with various SMC *Cre* driver mice, 90% of which were excised with several versions of *Tagln-Cre* or *Myh11-Cre* (Supplementary Table 1). Previous work with *Tagln-Cre* (aka *Sm22-Cre*) reported recombination in myeloid cell lineages.[31] For this reason, circulating cells (cleared of red blood cells) from tamoxifen-treated male and female *Itga8-CreER^{T2}* mice carrying the *mT/mG* reporter were isolated and compared to similarly prepared cells from tamoxifen-treated *Myh11-CreER^{T2}-mT/mG* male mice.[32] As expected, fluorescence-activated cell sorting revealed GFP positive circulating cells from an *Sm22-Cre* mouse[33]; however, essentially no GFP fluorescence was observed in circulating cells from *Itga8-CreER^{T2}* or *Myh11-CreER^{T2}* mice (Extended Data Fig. 3a). Moreover, analysis of bone marrow aspirates showed no activity of *Itga8-CreER^{T2}* or *Myh11-CreER^{T2}* in megakaryocytes or surrounding stromal cells (Extended Data Fig. 3b). Given the broad activity of *Sm22*-driven transgenes in cells of the vessel wall,[9] the balance of experiments were conducted in *Itga8-CreER^{T2}* and *Myh11-CreER^{T2}* mice only.

Itga8-CreER^{T2} showed preferential recombination in VSMCs

Confocal immunofluorescence microscopy was used to compare recombination activities across multiple tissues in age-matched *Itga8-CreER^{T2}* and *Myh11-CreER^{T2}* mice. Both strains demonstrated recombination activity in VSMCs of the aorta, mesentery, and microvasculature of the brain, as well as vessels in visceral organs such as intestine and bladder (Fig. 1a). Higher magnification, z-stacked images further confirmed recombination in VSMCs of the aorta and vena cava with no activity in endothelial or adventitial cells (Extended Data Fig. 4a,b). The activity of each *CreER^{T2}* driver was seen in VSMCs of the ascending aorta (mix of secondary heart field- and neural crest-derived VSMCs), aortic arch (neural crest-derived VSMCs), and thoracic/descending aorta (paraxial mesoderm-derived VSMCs) (Extended Data Fig. 4b). Confocal microscopy and immunogold electron microscopy demonstrated sporadic *Itga8-CreER^{T2}* activity in pericytes of the brain (Fig. 1b). Importantly, whereas *Myh11-CreER^{T2}* mice showed high recombination activity in visceral SMCs of bladder, colon, esophagus, intestine, stomach, and ureter, *Itga8-CreER^{T2}* mice displayed lower activity in these tissues, particularly intestine (Fig. 1a). Low *Itga8-CreER^{T2}* activity was also seen in the uterus (Fig. 1a); no comparison could be made in the uterus with *Myh11-CreER^{T2}* because this transgene integrated on the Y chromosome.[32] Comparable activity of *Itga8-CreER^{T2}* was observed in both male and female mice, whether derived from male or female *Itga8-CreER^{T2}* parents, up to the age of 54 weeks (Extended Data Fig. 4c), consistent with equivalent levels of ITGA8 protein in young versus old mice (Extended Data Fig. 4d). Neither *Itga8-CreER^{T2}* nor *Myh11-CreER^{T2}* mice displayed obvious activity outside of VSMCs in tissues of the eye, heart, pancreas, skeletal muscle,

spleen, and germ cells of the testis and ovary (Extended Data Fig. 5a,b). However, *Myh11-CreER^{T2}* mice exhibited pronounced activity in interstitial cells of the thymus, and *Itga8-CreER^{T2}* mice showed activity in glomerular cells of the kidney (Extended Data Fig. 5b). *Itga8-CreER^{T2}* activity was also detected in sinusoids of the liver, thecal cells surrounding mature follicles of the ovary, and in myoepithelial cells of the mammary gland (Extended Data Fig. 5b). Collectively, these results demonstrate some similarities, but important differences, in the recombination activities of *Itga8-CreER^{T2}* versus *Myh11-CreER^{T2}*.

Tamoxifen-independent activity and CreER^{T2} protein expression

There is evidence for tamoxifen-independent (or leaky) recombination in mice with the *CreER^{T2}* cassette.[34] Accordingly, individually-housed *Itga8-CreER^{T2}* or *Myh11-CreER^{T2}* male mice carrying the *mT/mG* reporter were analyzed for recombination in the absence of tamoxifen. Whereas no detectable recombination of the *mT/mG* reporter was noted in young *Itga8-CreER^{T2}* mice, clear evidence of tamoxifen-independent recombination was visible in similarly-aged tissues of *Myh11-CreER^{T2}* mice (Fig. 2a). There was no leaky activity in *Itga8-CreER^{T2}* mice up to 6 months of age suggesting high fidelity activity of this *CreER^{T2}* strain; however, low-level leaky recombination was seen in the aorta of 54-week-old *Itga8-CreER^{T2}* mice, although the extent of leakiness was much less than that of age-matched *Myh11-CreER^{T2}* mice (Extended Data Fig. 6). To begin probing the basis for early-onset leaky *Myh11-CreER^{T2}* activity, CreER^{T2} protein levels were analyzed in the aorta and bladder of age-matched young male mice. Western blotting showed five-fold greater CreER^{T2} protein in the aorta of *Myh11-CreER^{T2}* mice than *Itga8-CreER^{T2}* mice (Fig. 2b); higher levels of CreER^{T2} were seen in the bladder of *Myh11-CreER^{T2}* mice (Fig. 2b). In contrast, CreER^{T2} expression was undetectable in the bladder of *Itga8-CreER^{T2}* mice by Western analysis (Fig. 2b), although activity was evident with more sensitive confocal imaging (Fig. 1a). The level of *Myh11* mRNA expression is much higher than *Itga8* mRNA,[35] suggesting promoter strength may underlie differences in CreER^{T2} protein levels between the two strains. To further explore potential explanations for the differences in CreER^{T2} protein levels, Sanger sequencing of both *CreER^{T2}* drivers was carried out and the results disclosed a ~20% difference in nucleotide sequence (Supplementary Fig. 3). Close inspection of nucleotide differences revealed *Myh11-CreER^{T2}* to be codon optimized for more efficient translation of the bacterial Cre protein in mammals (Supplementary Fig. 3).[36] Moreover, quantitative PCR of genomic DNA from the *Myh11-CreER^{T2}* strain showed two copies of the transgene (Fig. 2c). The latter finding prompted efforts to physically map the *Myh11-CreER^{T2}* transgene using nanopore long read sequencing.[37] Interestingly, X chromosome-specific sequence near the pseudoautosomal region flanked the *Myh11-CreER^{T2}* transgene, suggesting initial integration on the X chromosome (Fig. 2d).

The higher expression of CreER^{T2} protein in *Myh11-CreER^{T2}* mice, and the unexpected presence of a segment of X chromosome sequence around the Y-integrated transgene,[32] suggested there could be perturbations in the vascular transcriptome of this *CreER^{T2}* driver strain. To investigate this idea, bulk RNA-seq studies were conducted and the results showed an altered transcriptome in the aorta of *Myh11-CreER^{T2}* and, to a lesser extent, *Itga8-CreER^{T2}* mice (Fig. 2e). Specifically, 101 upregulated genes (Group 1) and 323 down-regulated genes (Group 2) of *Myh11-CreER^{T2}* deviated further from wild type than

Itga8-CreER^{T2} (Fig. 2e). Interestingly, 40 genes (Group 3) upregulated in *Itga8-CreER^{T2}* aorta were down-regulated in *Myh11-CreER^{T2}* as compared to wild type aorta (Fig. 2e). Of note, there were no down-regulated genes unique to *Itga8-CreER^{T2}*. Consistent with there being two copies of the *Myh11-CreER^{T2}* transgene (Fig. 2c), two X-linked genes (*Arhgap6* and *Hccs*), found near the *Myh11-CreER^{T2}* insertion site (Fig. 2d), were expressed two-fold higher as compared to wild type and *Itga8-CreER^{T2}* aorta (Supplementary Table 2). Taken together, these results show several distinctive characteristics in the *Myh11-CreER^{T2}* driver strain including early, unscheduled recombination, high-level CreER^{T2} protein expression, and a more divergent baseline transcriptome likely driven, at least in part, by an unusual translocation event.

Similar recombination efficiencies between each *CreER^{T2}*

The differential expression of CreER^{T2} protein suggested there could be differences in recombination efficiency between the two *CreER^{T2}* driver strains. To address this possibility, *Myh11-CreER^{T2}* and *Itga8-CreER^{T2}* mice were crossed with several independently floxed mice to ascertain relative recombination rates. Quantitative PCR before and after tamoxifen administration showed comparable recombination of the *mT/mG* reporter in the aorta of both *CreER^{T2}* strains (Fig. 3a,b). As expected, there was high-level recombination in the intestine of *Myh11-CreER^{T2}* mice, but negligible amounts in *Itga8-CreER^{T2}* mice (Fig. 3a,b). Similar findings were observed in the bladder of a new tamoxifen-inducible *Myocardin* mouse model (Fig. 3c,d). Next, the activity of each *CreER^{T2}* strain was quantitated in popliteal lymphatic vessels. Results revealed ~90% and ~70% recombination efficiency in lymphatic vessels of the *mT/mG* reporter in *Myh11-CreER^{T2}* and *Itga8-CreER^{T2}* mice, respectively (Fig. 3e,f). Recombination efficiencies were somewhat lower in popliteal artery and vein, but the *Myh11-CreER^{T2}* activity appeared higher than *Itga8-CreER^{T2}* (Extended Data Fig. 7). Finally, each *CreER^{T2}* strain was crossed to a floxed *Srf* mouse[33] treated with oil or tamoxifen. Tamoxifen alone had no effect on the expression of SRF in wild type aorta (Extended Data Fig. 8a,b). Normalized SRF protein was similarly knocked down in the aorta of each *CreER^{T2}* strain; however, only *Myh11-CreER^{T2}* displayed significant knockdown of SRF in the bladder (Fig. 3g,h). Overall, despite lower expression of CreER^{T2} protein in *Itga8-CreER^{T2}* mice, excision of floxed sequences approximated that seen in *Myh11-CreER^{T2}* mice.

Itga8-CreER^{T2}-mediated *Srf* knockout evades lethal visceral myopathy

Srf loss-of-function studies using a *Sm22-CreER^{T2}* driver showed a fatal gastrointestinal phenotype.[10, 11] Consistent with these findings, tamoxifen-treated homozygous floxed *Srf* mice carrying *Myh11-CreER^{T2}* (*Srf^{Myh11}*) displayed lethality beginning three weeks following the first tamoxifen injection. Mutant mice showed a pale, distended intestine and a pronounced reduction in SRF expression within a thinned muscular layer of the small intestine (Extended Data Fig. 8c,d). In contrast, inducible knockout of *Srf* with *Itga8-CreER^{T2}* (*Srf^{Itga8}*) resulted in viable mice with no intestinal phenotype up to eight weeks post-tamoxifen administration (Extended Data Fig. 8c). Confocal immunofluorescence microscopy demonstrated a clear reduction of SRF and ACTA2 in the carotid artery of *Srf^{Itga8}* mice, but not in bladder or intestinal SMCs (Extended Data Fig. 9a). Quantitative measures disclosed a ~75% decrease in SRF positive VSMCs in the carotid artery with little

change in the intestine (Extended Data Fig. 9b,c). Western blot studies indicated a similar diminution of SRF in homozygous floxed (HoF) *Srf*^{Itga8} knockout aorta, but no significant change in the bladder (Extended Data Fig. 9d-g). There was little change in SRF expression in the aorta of heterozygous floxed (HeF) *Srf*^{Itga8} mice, suggesting compensatory expression from the remaining wild type allele (Extended Data Fig. 9d,f).

Because *Itga8-CreER*^{T2} activity was seen in the glomerulus (Extended Data Fig. 5b), conditional loss of *Srf* with this *CreER*^{T2} driver could have triggered a kidney phenotype. We therefore analyzed homozygous and heterozygous *Srf*^{Itga8} mice for pathological changes in the kidney. Results revealed similar body weights, a normal histological appearance, and no indication of proteinuria in *Srf*^{Itga8} mice (Supplementary Fig. 4). Taken together, these results support *Itga8-CreER*^{T2} as a suitable alternative to *Myh11-CreER*^{T2} in focused studies of *Srf* loss-of-function in VSMCs, without the confounding effects of an otherwise lethal visceral myopathy.

Vascular dysfunction in *Itga8-CreER*^{T2}-mediated *Srf* knockout mice

To formally establish an unambiguous phenotype associated with *Srf* gene loss in VSMCs, blood pressure and vascular contractile competence were assessed in male and female mice following *Itga8-CreER*^{T2}-mediated knockout of *Srf* (*Srf*^{Itga8}). Telemetry measures in male mice demonstrated no change in baseline blood pressure. However, following angiotensin II infusion, significant increases in systolic, diastolic, and mean arterial pressures were observed in control mice, but not in *Srf*^{Itga8} mice (Fig. 4). Consistent with a previous report,[38] age-matched female mice failed to respond to angiotensin II and showed no changes in blood pressure, regardless of *Srf* status (Fig. 5). On the other hand, the aorta of male and female mice displayed attenuated contraction in response to KCl (Fig. 6a) and phenylephrine (Fig. 6b,c). Immunofluorescence confocal microscopy of the aorta from *Srf*^{Itga8} mice indicated attenuated expression of SRF and ACTA2 in VSMCs (Fig. 6d). Similarly reduced SRF and contractile protein expression was seen in mesenteric arteries (Extended Data Fig. 10). Finally, bulk RNA-seq studies established a decrease in VSMC contractile genes in the aorta of *Srf*^{Itga8} mice (Fig. 7a,b). Analysis of the top 250 down-regulated genes disclosed the SRF binding CArG box as the most significantly enriched *cis* regulatory element (Fig. 7c). Further assessment of the down-regulated gene set showed molecular functions related to the cytoskeleton and contractile machinery (Fig. 7d). Interestingly, the upregulated gene set in *Srf*^{Itga8} aorta was most related to metabolism (Fig. 7e). Collectively, these results demonstrate an unambiguous viable mouse model of VSMC contractile incompetence following *Itga8-CreER*^{T2}-mediated inactivation of *Srf*.

Discussion

All current SMC *Cre* driver mice recombine floxed DNA similarly in both vascular and visceral SMC lineages. Consequently, the inactivation of a critical gene in SMCs of the intestine, for example, may result in a lethal phenotype and the inability to accurately define gene function in VSMCs. Here, preferential activity of *Itga8-CreER*^{T2} was demonstrated in VSMCs with relatively less activity in visceral SMCs of the gastrointestinal and urinary tracts. Such restricted CreER^{T2} activity resulted in viable mice upon inactivation of *Srf*

with no gross or histological evidence of pathology in the intestine. These findings are consistent with *mT/mG* reporter data and quantitative experiments showing similar levels of SRF protein in intestinal SMCs of wild type and Srf^{Itga8} mice. In sharp contrast, *Srf* loss-of-function with the *Myh11-CreER*^{T2} driver provoked a lethal intestinal phenotype; a similar finding was reported previously with suppression of SRF-dependent pro-survival microRNAs and resultant intestinal SMC apoptosis.[39] The latter phenotypes and the intestinal pseudo-obstruction seen with conditional knockout of *Srf* using an inducible *Sm22-Cre* driver[10, 11] have hampered efforts to study *Srf* loss-of-function in VSMCs, particularly in models that require extended time for disease to be evident. Importantly, despite much lower levels of CreER^{T2} protein as compared to the *Myh11-CreER*^{T2} driver, *Itga8-Cre*ER^{T2} efficiently recombined the floxed *Srf* locus revealing an unequivocal VSMC phenotype of contractile incompetence. Based on the results of this study, the *Itga8-CreER*^{T2} mouse would be expected to circumvent other lethal visceral myopathies following gene loss with existing SMC *Cre* drivers.

Although short-term (14-15 days) studies of conditional loss of *Srf* in VSMCs with *Sm22-CreER*^{T2} have been reported, yielding insight into mechanosensitivity and blood flow[40] as well as arterial stiffness,[41] phenotyping occurred at a time when dilation of the intestine, defective peristalsis, and cachexia begin to be manifest.[10, 11] The latter changes likely elicited systemic inflammation that could impact vascular function. As shown here, angiotensin II-induced increases in systemic blood pressure were abolished in male mice lacking normal levels of SRF indicating the phenotype was solely due to an intrinsic defect in VSMCs with no contribution from distal pathological events. Thus, future *Srf* loss-of-function studies can now be conducted in VSMCs without the confounding effects of early onset gastrointestinal defects or other visceral pathologies. Further, we anticipate that the *Itga8-CreER*^{T2} mouse will find utility as more floxed alleles emerge for studies in acute vascular disease models of intimal hyperplasia and chronic models such as arteriovenous fistula failure, atherosclerosis, hypertension, transplant arteriopathy, and arterial calcification.

A limitation of some *Cre* driver strains is the recombination of a floxed allele in the absence of tamoxifen.[34] Here, the *Itga8-CreER*^{T2} mouse showed high fidelity recombination up to six months of age. In contrast, tamoxifen-independent *Myh11-CreER*^{T2} activity was evident in multiple tissues, including aorta, as early as 10 weeks of age. Such unscheduled recombination was more apparent in aged mice. A similar finding of tamoxifen-independent *Myh11-CreER*^{T2} activity was reported in SMCs of the stomach.[42] These findings should alert investigators as to the best controls for inducible knockout studies. For example, in the absence of haploinsufficiency and no leaky CreER^{T2} activity, a stringent control would be tamoxifen-administered mice carrying *CreER*^{T2} and a heterozygous floxed allele. If, however, haploinsufficiency is suspected and/or the *CreER*^{T2} driver is leaky, then a less confounding control would be tamoxifen-treated mice carrying *CreER*^{T2} without *lox*P sites.[43] Of note, there has been a suggestion that “pseudo *lox*P sites” in the genome could be subject to Cre-mediated recombination with unknown consequences.[44] Clearly, careful analysis of a *CreER*^{T2} driver and the expression profile of floxed alleles is essential when contemplating a conditional knockout experiment.[45]

What is the basis for the precocious leaky activity seen in the *Myh11-CreER^{T2}* driver? One possibility could be the comparatively greater amounts of CreER^{T2} protein observed in this strain. Indeed, in vitro studies have correlated tamoxifen-independent activity with higher levels of CreER^{T2} protein.[46] An overabundance of CreER^{T2} protein may favor dissociation from the HSP90 chaperone, which anchors CreER^{T2} in the cytoplasm thereby preventing CreER^{T2} entry into the nucleus in the absence of ligand.[47] The finding of two copies of the *Myh11-CreER^{T2}* transgene and, perhaps, stronger *Myh11* promoter activity over *Itga8*, likely contribute to the high-level CreER^{T2} protein observed in *Myh11-CreER^{T2}* mice. Theoretically, only four molecules of Cre are needed per cell to catalyze recombination between two *lox*P sites.[48] Thus, the weak expression of CreER^{T2} demonstrated here in the *Itga8-CreER^{T2}* mouse has distinct advantages over the *Myh11-CreER^{T2}* strain by effecting comparable recombination efficiencies while displaying low-level leakiness observed only in mice greater than six months of age.

Another advantage of the *Itga8-CreER^{T2}* mouse is the ability to perform sex studies which enables compliance with the National Institutes of Health directive of addressing sex as a biological variable in biomedical research.[49] The present *Myh11-CreER^{T2}* mouse carries the *CreER^{T2}* allele on the Y chromosome, precluding studies in females.[9] A previous study reported translocation of *Myh11-CreER^{T2}* to the X chromosome and the generation of female mice that displayed some *Myh11-CreER^{T2}* activity.[50] It should be pointed out, however, that the site of integration on the X chromosome was not mapped, and high doses of tamoxifen were needed to elevate recombination efficiency in hemizygous females.[50] Here, using nanopore long-read sequencing,[37] the *Myh11-CreER^{T2}* transgene was physically mapped in a male mouse. Results suggest that the transgene initially integrated at the terminal end of the X chromosome near the pseudoautosomal region where high rates of recombination occur during meiosis.[51] The *Myh11-CreER^{T2}* transgene then translocated to the Y chromosome carrying at least two X-linked genes, which are more abundantly expressed in *Myh11-CreER^{T2}* mice than wild type or *Itga8-CreER^{T2}* mice. The precise insertion site on this “neo Y chromosome” remains unclear, but it must be within an interval between the pseudoautosomal region and the pseudoautosomal boundary (where identical X and Y sequences diverge) to explain the ~3% of *Myh11-CreER^{T2}* t(Y;X) mice observed in this lab over the last five years. This peculiar site of integration suggests several substrains of the original *Myh11-CreER^{T2}*[32] driver may exist due to stochastic recombination and probable variation in breakpoints. Future engineering of *Cre* (or other recombinase) mice should use a more targeted approach for single copy integration, either within a gene of interest or a safe harbor locus on an autosome. Given early unscheduled recombination with *Myh11-CreER^{T2}*, the unusual translocation events associated with its site of integration, and the high level activity in visceral SMC tissues, there is an opportunity to revisit previous conclusions drawn from the >100 alleles targeted in SMCs with this *CreER^{T2}* driver (Supplementary Table 1).

Despite the *Itga8-CreER^{T2}* mouse enabling sex studies in a more VSMC-restrictive manner without leaky activity up to at least six months of age, some limitations need comment. First, as loss of both functional *Itga8* alleles is lethal,[30] breeding the *Itga8-CreER^{T2}* mouse to homozygosity is pointless. Indeed, breeding any unmapped transgenic line to homozygosity is ill-advised since randomly integrated transgenes may disrupt critical coding or noncoding

genes or essential regulatory elements.[52] Second, *Itga8* appears to be down-regulated under conditions of SMC de-differentiation,[27] so the *Itga8-CreER^{T2}* driver may not be optimal for studies requiring inducible activity following disease onset, although there is evidence for the up-regulation of ITGA8 protein late in intimal disease.[53] Further work in various vascular disease models will resolve this issue. Third, the activity profile of *Itga8-CreER^{T2}* during embryogenesis was not assessed, so it is unclear whether this *CreER^{T2}* driver will be suitable for developmental studies. Fourth, low *Itga8-CreER^{T2}* activity in uterine SMCs suggests this *CreER^{T2}* driver may not be useful for studying effects of conditional SMC gene loss in the female reproductive tract. Fifth, whether *Itga8-CreER^{T2}* is active in other SMC types such as those in arrector pili of skin and ciliary body of the eye remains to be determined. Finally, as with all current SMC *Cre* drivers, *Itga8-CreER^{T2}* exhibits activity in non-SMC types, most notably glomerular cells of the kidney. Thus, when using the *Itga8-CreER^{T2}* mouse for conditional knockouts, it may be necessary to assess kidney function through histological and biochemical assays.[54] In this report, *Srf^{Itga8}* mice exhibited normal glomerular and tubular structures with no evidence of proteinuria. Whether a kidney phenotype is manifest under stress conditions awaits further study. Further, since there is some level of *Itga8-CreER^{T2}* activity in visceral SMCs (Fig. 1a), it will be important to determine whether gene-specific phenotypes exist in these tissues under certain experimental conditions.

In addition to glomerular cells, *Itga8-CreER^{T2}* activity was observed in sinusoidal cells of the liver where endothelial cells and fibroblast-like stellate cells reside; only occasional liver sinusoidal activity was seen with *Myh11-CreER^{T2}*. Given a previous report of ITGA8 in stellate cells,[55] the lack of *Itga8-CreER^{T2}* activity in vascular endothelial cells as reported here, and the virtual absence of *Itga8* mRNA expression in various endothelial cell populations,[35] the activity of *Itga8-CreER^{T2}* in liver sinusoids likely occurs in stellate cells. Of note, no obvious *Itga8-CreER^{T2}* activity was observed in cardiac fibroblasts or adventitial fibroblasts of blood vessels. Whether activity emerges in these and other fibroblast populations under stress conditions is unknown at this time. While no *Itga8-CreER^{T2}* activity was detected in resting endothelial cells, activity may arise under conditions of endothelial-mesenchymal transition or in unique endothelial cell beds as reported for *Myh11-CreER^{T2}*.[56] *Itga8-CreER^{T2}* activity was also demonstrated in myoepithelial cells of the mammary gland and thecal cells encapsulating mature follicles of the ovary. We do not anticipate gene loss in the aforementioned non-SMC types to impact a VSMC phenotype. Nevertheless, investigators should be mindful of the full expression profile of a floxed gene to probe potential competing phenotypes outside the vascular or lymphatic vessel wall when using the *Itga8-CreER^{T2}* mouse. Continued characterization of *Itga8-CreER^{T2}* under various experimental conditions will provide further insight into its activity profile.

An ongoing question in vascular biology is whether SMC *Cre* drivers are active in pericytes, an SMC-like cell that is essential for maintaining capillary integrity and function.[57] A previous report found *Myh11-CreER^{T2}* activity in pericytes of the retina, cornea, and hindlimb skeletal muscle.[58] In contrast, only an occasional pericyte of the brain showed evidence of *Itga8-CreER^{T2}* activity, a finding consistent with an analysis of *Itga8* mRNA expression in single-cell RNA sequencing of the mouse brain.[35] Thus, interrogating *Srf* loss-of-function phenotypes in pericytes using the *Itga8-CreER^{T2}* driver may be uninformative.

Recently, however, an elegant study using *Pdgfrb-CreER^{T2}* to disrupt *Srf* in pericytes found defective migration of these cells during sprouting angiogenesis in the newborn retina resulting in faulty vascular remodeling, aberrant blood flow patterns, and the formation of arteriovenous shunts.[59] Table 1 summarizes notable distinctions between *Itga8-CreER^{T2}* and *Myh11-CreER^{T2}* mice.

Little is known about the transcriptional/post-transcriptional control of *Itga8*. In vitro luciferase and transgenic mouse assays failed to show the importance of a conserved SRF-binding site located four kilobases upstream of the start site of *Itga8* transcription.[29] However, the Myocardin (MYOCD) coactivator stimulated *Itga8* expression in an SRF-independent manner.[29] The latter finding distinguishes *Itga8* from most other SMC markers that have functional SRF-binding sites in the promoter or first intron.[60] Elucidating the transcriptional control of *Itga8* and other VSMC-restricted genes will inform the molecular basis for preferential expression in VSMCs and the further development or refinement of *Cre* driver mice for VSMC conditional knockout studies.

In summary, the *Itga8-CreER^{T2}* mouse displays preferential activity in VSMCs, an attribute that has yet to be shown in any existing SMC-restricted *Cre* driver. As such, the *Itga8-CreER^{T2}* mouse represents a solution to the problem of competing, sometimes lethal, phenotypes arising from the inactivation of critical genes in visceral SMCs such as the intestine.

Methods

Mouse models

All mouse studies were approved by local Institutional Animal Care and Use Committees at the University of Rochester during the period of 2016-2019 (approval #101587); Medical College of Georgia from 2019-present (approval number #2019-1000); and the University of Missouri (approval #27320). An Institutional Biosafety Committee at Augusta University approved the use of Tamoxifen for inducible activation of relevant *Cre* driver mice (approval #1942). The ethical treatment of mice was in accordance with ARRIVE guidelines. All mice were maintained in micro-isolator cages containing water and pelleted food (Teklad Global Irradiated 18% Protein Rodent Diet 2918) *ad libitum*. Rooms were temperature and humidity controlled under a 12-hour light (600-1800 hours), 12-hour dark (1800-600 hours) cycle. The *Myh11-CreER^{T2}* mouse (stock 019079) and membrane tdTomato/membrane GFP (*mT/mG*) reporter (stock 007676) were obtained from the Jackson laboratory. The *Sm22-Cre* and floxed *Srf* strains have been described previously.[33] To generate the *Itga8-CreER^{T2}* allele, a DNA fragment containing *CreER^{T2}-P2A-mCherry* coding sequence and SV40 polyadenylation signal (*CreER^{T2}-P2A-mCherry-pA*) was synthesized by GENEWIZ. A 0.7-kb 5'-homology arm comprising promoter and untranslated exon 1 of *Itga8* and a 1.1-kb 3'-homology arm containing the coding sequence of exons one and two, intron one, and a portion of intron two of *Itga8,* were PCR-amplified from C57BL/6J genomic DNA (primers listed in Supplementary Table 4). The homology arms were cloned, along with an FRT flanked pGK-Neo, pGK-DTA, and *CreER^{T2}-P2A-mCherry-pA* cassette, into pBluescript SKII (+) to generate the *Itga8-CreER^{T2}* knock-in construct (Extended Data Fig. 1). The targeting construct was linearized with *AscI* and electroporated into C57BL/6J-129S6

hybrid G4 embryonic stem cells (ESCs).[61] The targeted *Itga8-CreER^{T2}* ESC clones were confirmed by long and accurate PCR genotyping using external primers to identify the 1.0 kb 5' and 1.3 kb 3' targeted DNA fragments (primers listed in Supplementary Table 4). Validated ESCs were microinjected into C57BL/6J blastocysts to generate mouse chimeras. By crossing the chimeras with FLPeR mice in C57BL/6J background (Jackson Laboratory, 009086), the *Neo* cassette was removed to produce the *Itga8-CreER^{T2}* mouse line. Sanger sequencing both strands verified the final knockin allele. *Itga8-CreER^{T2}* activity was assessed in early (N2-N3) and later (>N10) generation mice of age 8-12 weeks (unless specified otherwise) and were maintained strictly on a C57BL/6J background with continuous refreshing of the breeder colony every fifth generation to mitigate effects of genetic drift and inadvertent generation of a substrain. Older *Itga8-CreER^{T2}* (24 and 54 weeks) and *Myh11-CreER^{T2}* (54 weeks) mice, each carrying the *mTmG* reporter, were used to evaluate tamoxifen-independent activity during aging. The inducible *Myocd* mouse (iMyocd) was generated in the same ESC line as above with an HA-tagged *Myocd* cDNA cloned downstream of a CAG-driven stop-floxed cassette in the *Rosa26* locus. A list of mouse models used in this report is provided in Supplementary Table 3.

Tamoxifen administration

Cre mouse lines were crossed with *mT/mG* fluorescent reporter mice, a floxed *Srf* mouse, or an inducible *Myocd* mouse. Inducible *Cre* activity was achieved by intraperitoneal injection of tamoxifen (Sigma-Aldrich, T5648) mixed and sonicated in 100% ethanol/sunflower seed oil (Sigma-Aldrich, S5007) at 1:9, v/v. Tamoxifen (40 mg/kg) was delivered daily over five days followed by a washout of at least 10 days before experimental measures.

Confocal microscopy

For frozen samples, fresh tissues were rapidly isolated and fixed overnight in 4% paraformaldehyde. Tissues were then cryoprotected over a second night with 30% sucrose followed by embedding in Optimal Cutting Temperature (OCT) compound (VWR, 102094-106). 5μm-7μm sections were cut with a cryostat (Leica Biosystems, CM 1950) and kept frozen until imaging. Slides were removed from −20°C and warmed to room temperature. OCT compound was removed by washing three times with 1x PBS. Auto-fluorescence was quenched with Vector® TrueVIEW® Autofluorescence Quenching Kit (Vector Laboratories, SP-8500-15) and the slides were cover-slipped with ProLong™ Gold Antifade Mountant (Thermo, P36930) containing DAPI stain and air-dried. Imaging was performed by a single person (OJS) who was blinded to the genotype for all images shown (save Fig. 3e and Extended Data Fig. 7) on either an Olympus IX81 or Zeiss LSM900 confocal microscope with 20x, 40x oil (z-stacked), and 60x oil (z-stacked) objectives and analyzed with Micro-manager 2.0 or ZEN 3.5 Blue software, respectively. Laser settings for confocal imaging were kept constant throughout. Final images were cropped to their published size in Adobe® Photoshop® with no digital enhancements, save the Testis panel corresponding to *Itga8-CreER^{T2}* in Extended Data Fig. 5a and the *Itga8-CreER^{T2}* data of Extended Data Fig. 6; the brightness was increased uniformly in each of these panels using Photoshop® to provide the reader with a better representation of GFP staining.

For paraffin sections, tissues were isolated and immersion-fixed in methanol-H_2O-acetic acid (60/30/10, v/v) overnight, processed in a benchtop tissue processor (Leica Biosystems, TP1020), and embedded (Sakura, Tissue Tek TEC 5) in paraffin blocks. Sections were cut with a microtome (Microm, HM 355 S) at 5μm and baked overnight at 58°C. Slides were then deparaffinized in a Leica® Autostainer XL (Leica Biosystems, ST5010), stained with antibodies (Supplementary Table 5), quenched with Vector® TrueVIEW® Autofluorescence Quenching Kit (Vector Laboratories, SP-8500-15), and cover-slipped with ProLong™ Gold Antifade Mountant. Imaging was done on an Olympus IX81 or Zeiss LSM900 confocal microscope with 20x, 40x oil (z-stacked), and 60x oil (z-stacked) objectives and analyzed with Micro-manager 2.0 or ZEN 3.5 Blue software, respectively. Final paraffin sectioned images were processed in Photoshop® without any enhancements.

Assessment of *Itga8-CreER^{T2}/mTmG* recombination in cerebral pericytes

Itga8-CreER^{T2}/mTmG mice were induced with tamoxifen and anesthetized as described above. Once an anesthetic plane was reached, 200 μl of wheat germ agglutinin-AF647 (AlexaFluor-647; WGA-647 W32466 ®Fisher), suspended in sterile saline at 1mg/ml, was injected into the retroorbital sinus for five minutes for WGA-647 to distribute throughout the vasculature and bind to the endothelial glycocalyx. After five minutes, the mouse was euthanized by cervical dislocation and the brain removed from the skull. Sagittal slices of the brain were made with a razor blade and placed in Krebs buffer with 0.5% BSA. A piece of Sylgard 184® was used to weigh the brain slice against the coverslip bottom of a WPI FluoroDish Cell Culture Dish to prevent movement while imaging. We scanned the tissue for GFP^+ cells that displayed the canonical pericyte morphology and acquired image stacks for tdTomato, GFP and WGA-AF647 with a Z-step of 0.33μm using a Leica 25x water objective (HC FLUOTAR L 25x/0,95 W VISIR) and an Andor Dragonfly scanning confocal head with a LEICA DMi8 inverted microscope. The color intensity and balance were uniformly adjusted to minimize brain autofluorescence and to highlight the *Itga8-CreER^{T2}* mediated GFP expression. Maximum projections were made using Fiji.[62]

Immunogold electron microscopy

Mice were perfusion fixed with 4% paraformaldehyde/2% glutaraldehyde in 0.1M cacodylate buffer (pH, 7.4), dissected and immersion fixed in the same fixative, dehydrated through a graded series of ethanol, and embedded in LR White Resin (Electron Microscopy Sciences [EMS], Ft. Washington, PA). Following facing and trimming of block, 75 nm sections were collected on Pioloform-coated nickel slot grids (Ted Pella, Redding, CA), floated on drops of etching solution (5% $NaIO_4$ in PBS) for five minutes, washed in PBS, and then quenched for 30 minutes in 1M NH_4Cl. Grids were blocked in Aurion Blocking Solution (EMS) for two to four hours at room temperature, floated on drops of rabbit anti-GFP (Novus Biologicals, Centennial, CO) at a dilution of 1:1000 overnight at 4°C and then washed in PBS. Grids were then floated on drops of anti-rabbit Nanogold (Nanoprobes, Yaphank, NY) reagent diluted 1:1000 in Aurion BSA-c buffer for three hours at room temperature. Nanogold particles were silver enhanced for 15 minutes using HQ Silver (Nanoprobes, Yaphank, NY), washed in ice-cold deionized water to halt enhancement, and stained with 2% uranyl acetate and lead citrate. Images were obtained with a JEOL

1400 Flash transmission electron microscope (JEOL USA Inc., Peabody, MA) at 120 kV, equipped with a One View CCD camera (Gatan Inc., Pleasanton, CA).

Recombination efficiency

Floxed mouse models carrying either *Itga8-CreER^{T2}* or *Myh11-CreER^{T2}* were treated with oil or tamoxifen as above. Following a standard 10-day washout period, tissues (aorta and intestine) were isolated for quantitative PCR of genomic DNA (*mT/mG* reporter) and Western blotting for the inducible *Myocardin* and floxed *Srf* mice, respectively. For popliteal vascular recombination efficiencies, mice were anesthetized with an injection of ketamine/xylazine (25/2.5 mg/ml, i.p.) and their legs shaved and cleaned. The popliteal artery and vein and the popliteal lymphatic vessel were excised from the tissue and kept in Krebs buffer with 0.5% BSA at 4°C until imaged. Each vessel was then cannulated and pressurized in an imaging chamber filled with Krebs buffer for further removal of adipose and connective tissue. Vessels were then equilibrated in calcium-free solution for 15 minutes to prevent movement during live imaging. At least two separate fields of view of each vessel were acquired with a Yokogawa CSU-X Spinning Disc Confocal Microscope on an inverted Olympus IX81 with a Hamamatsu Flash4 camera using both 20x and 40x objectives. Each live vessel acquisition was a Z-stack from the bottom edge of the vessel to the approximate midpoint for both the membrane GFP (488nm) and membrane tdTomato wavelengths (561nm). In Extended Data Fig. 7, maximum image projections from live popliteal artery and vein vessels were created from a confocal microscopy image stack using Fiji and the Z-Project Function. The resulting maximum projection was cropped to its final size, and intensity for each channel was adjusted across both image sets using Fiji to highlight GFP fluorescence due to *ITGA8-CreER^{T2}* activity. For the representative vessel stitching, the Fiji plugin for pairwise stitching was used to stitch three fields of view, acquired at 20x, together.[63]

Following the live image acquisition, the lymphatic popliteal vessels were fixed at room temperature with ice-cold 4% PFA for 15 minutes. The vessels were then washed with PBS and stored at 4°C for subsequent immunostaining. The fixed vessels were permeabilized with PBST (0.3% triton) for one hour and then blocked for three hours with BlockAid (Thermofisher). Vessels were stained overnight with anti-GFP at 1:200 (rabbit, ThermoFisher A-11122) and anti-smooth muscle actin (ACTA2) at 1:500 (mouse, Sigma A5228) in Blockaid buffer. The vessels were then washed with PBS and stained with Donkey anti-rabbit AF488 (A-21206, Thermofisher) and Donkey anti-mouse AF647 at 1:200 (A-31571, Thermofisher) for one hour at 4°C. Vessels were washed in PBS and then recannulated and imaged as described above.

To assess recombination efficiency in the smooth muscle layer of the popliteal vein and artery, the number of circumferential VSMCs expressing either GFP$^+$ or tdTomato$^+$ were tabulated from Z-stacks from 40x acquisitions. To assess recombination efficiency in the smooth muscle layer of popliteal lymphatic vessels the number of GFP$^+$/ACTA2$^+$ and GFP$^-$/ACTA2$^+$ lymphatic muscle cells were counted and tabulated from Z-stacks acquired at 40x. To create the differential images used as a visual aid, the RFP Z-stack and GFP Z-stack were converted to 32-bit images, the RFP Z-stack was divided by the GFP Z-stack in FIJI and a

maximum projection was made of the resulting stack. The output image was merged with the GFP maximum projection and the threshold was adjusted to highlight the GFP negative but ACTA2 (SMA) positive cells in FIJI.

Western blotting

Harvested cells or pulverized frozen tissues were washed with cold 1x PBS and lysed with RIPA Buffer (Sigma, R0278) containing complete protease inhibitor cocktail (Sigma-Aldrich, 4693132001). Protein concentration was determined (Bio-Rad, 5000202) and samples were boiled with NuPAGE LDS buffer (Thermo, NP0008). Samples were run in 4-20% SDS-PAGE gel (Bio-Rad, 4561094) in 1x Tris-Glycine running buffer (Bio-Rad, A0028). Proteins were transferred to PVDF membrane using Trans-blot Turbo transfer system and compatible transfer kit (Bio-Rad, 1704272). Membranes were blocked in blocking buffer (Bio-Rad, 12010020) and incubated with appropriate antibodies (Supplementary Table 5). Antibodies were validated by the respective providers for the applications described here; SRF and ITGA8 antibodies were further validated in the lab by loss-of-function and inclusion of positive/negative control tissues, respectively. Finally, chemiluminescent substrate (Bio-Rad, 1705061) and ChemiDoc imaging system (Bio-Rad, 120031) were used for digital imaging of Western blots. Molecular weight markers reflect the approximate size of proteins in kilodaltons. Urine from homozygous Srf^{Itga8} and heterozygous Srf^{Itga8} mice was collected and denatured in NuPAGE LDS buffer. Samples were loaded onto an SDS-PAGE gel and run in 1x Tris-Glycine running buffer. Gels were stained with Coomassie blue and images were documented as above. Purified bovine serum albumin was run alongside the urine samples and served as a positive control for the presence of protein.

RNA isolation and real-time quantitative RT-PCR

Total RNA was extracted using QIAzol® Lysis Reagent (Qiagen, 79306) followed by isopropanol precipitation and 70% ethanol washing. GlycoBlue™ Coprecipitant was applied for single aorta to facilitate the handling of small quantities of RNA. Air-dried RNA pellets were dissolved in RNase-free water. Reverse transcription was performed using Bio-Rad iScript cDNA synthesis kit (Bio-Rad, 1708891) after DNase I treatment (Thermo, AM2222). Real time quantitative PCR was performed using iTaq Universal SYBR Green Supermix (Bio-Rad, 1725121) with primers listed in Supplementary Table 4. Following delta delta Ct normalization to a housekeeping control, levels of normalized gene expression were plotted as fold-change from control samples.

Bulk RNA-seq

Homozygous Srf^{Itga8} and heterozygous Srf^{Itga8} mice (n=3 mice each) were administered tamoxifen at six weeks of age as above. Four weeks after the first dose of tamoxifen, aortas were collected and homogenized in RNeasy Plus Micro Kit with genomic DNA eliminator columns (Qiagen, 74034). Total RNA library preparation (TruSeq stranded) and high-throughput RNA-seq were performed on an Illumina HiSeq 4000 by Genomics Research Core of the University of Rochester. Gene Ontology analysis was done with DAVID (https://david.ncifcrf.gov/) and over-representation of transcription factor binding sites was determined with oPOSSUM.[64] In a separate experiment, aortas from male wild

type mice or age-matched mice with either *Itga8-CreER*^{T2} or *Myh11-CreER*^{T2} (n=3) were processed for total RNA isolation, library preparation, and sequencing on the Illumina NovaSeq 6000 at the University of Rochester. Standard data analysis, including principal component analysis and differential gene expression were done as described previously at the University of Rochester Genomics core.[65]

Nuclear-cytoplasmic RNA fractionation for LncRNA expression

Cultured mouse vascular smooth muscle cells (MOVAS) were fractionated using Protein and RNA isolation system kit according to the manufacturer's protocol (Thermo Fisher, AM1921). A list of cell lines used is provided in Supplementary Table 6. Real-time qRT-PCR was done with primers to the LncRNA upstream of *Itga8* as well as *Actb* primers, used as a cytoplasmic marker (Supplementary Table 4).

Flow Cytometry

Whole blood samples were collected from wild type, *mTmG*, *Myh11-CreER*^{T2}*/mTmG*, *Sm22-Cre/mTmG,* and *Itga8-CreER*^{T2}*/mTmG* mice and centrifuged for five minutes at 2000x g at room temperature. Buffy coats were carefully transferred to a fresh 1.5ml microfuge tube. 500ul of 1x ACK Lysing Buffer (Thermo, A1049201) was added to lyse red blood cells. Samples were then centrifuged for five minutes at 3000x g at room temperature. Supernatants were carefully aspirated and the pellets were suspended in 1x PBS. Cell suspensions were analyzed using an Accuri C6 flow cytometer (BD Biosciences) in the Flow Cytometry Core of the University of Rochester. Signals from the FITC channel were collected and gated for GFP-positive cells from each experimental condition. Please see Supplementary Fig. 5 and the Reporting Summary for more details.

Radio-telemetry recording of blood pressure

All physiological studies used male and female mice homozygous for floxed *Srf* and heterozygous for *Itga8-CreER*^{T2} (± tamoxifen). Following a 10-day washout period from the last tamoxifen (or oil) injection, male and female mice (13 weeks) were implanted with indwelling telemeters (carotid catheter) (DSI© Model #PA-C10, New Brighton, MN) under isoflurane anesthesia as previously described.[66] After a seven day recovery period, baseline blood pressure (BP; mean arterial pressure, systolic and diastolic pressure) and heart rate measurements were consciously recorded for seven days. Mice were then implanted with subcutaneous mini-osmotic pumps (Alzet, model 1002, 14-day pump 0.25 ul/hour) containing angiotensin II (Phoenix Pharmaceuticals) diluted in isotonic saline at a dose of 490ng/kg/min as previously described.[67] Blood pressure was recorded subsequently for 14 days.

Vascular Reactivity

Thoracic aortas from mice utilized for telemetry blood pressure recording protocol (ANGII-infused) were excised and cleaned of excess adipose tissue. Aortas were cut in 2mm rings and mounted on pins of a DMT® wire myograph (Ann Arbor, MI) as previously described.[66] Concentration response curves to phenylephrine (1nM −30μM concentrations) as well as

maximum responses to KCl (80mM) were performed and recorded with LabChart® analysis software (AD Instruments®, Colorado Springs, CO).

Mapping and copy number determination of *Myh11-CreER^{T2}*

Long-read libraries of (i) Ultra-Long DNA Sequencing (SQK-ULK001) and (ii) Cas9 Sequencing (SQK-CS9109) kits from ONT Nanopore were prepared following the manufacturer's instructions (www.nanoporetech.com). For Ultra-Long DNA libraries, ultrahigh molecular weight genomic DNA was isolated with Circulomics kits (NB-900-601-01 and NB-900-701-01) following the manufacturer's instructions (www.circulomics.com). For Cas9 libraries, high molecular weight genomic DNA was isolated with an NEB kit (T3060) following the manufacturer's instructions (www.neb.com). Five males, including a male from Jackson Laboratory (www.jax.org/), were used as input for mapping as described.[68] For Cas9 Sequencing (CRISPR-LRS),[68] crRNAs were designed with CHOPCHOP using default parameters (https://chopchop.cbu.uib.no) (Supplementary Table 4). Long-read libraries were run on R9.4.1 flow cells on a minION Mk1B or a GridION Mk1 with fast5 to fastq read conversion using guppy (v4.2.2) on MinKNOW (v20.10.3) MinKNOW Core (v4.1.2) and fast base-calling option for the base-call model and minimum Q-score of 7 option for read filtering. Fastq files were mapped to reference sequences (improved *Cre* or segments of chromosome 16) using the Long-Read Support (beta) plugin in Qiagen CLC Genomics Workbench (www.qiagen.com) which uses open-source tool minimap2. Mapped, informative reads were manually queried against NCBI nr/nt, Refseq genome databases (https://blast.ncbi.nlm.nih.gov/Blast.cgi) and UCSC genome browser with BLAT tool (https://genome.ucsc.edu), where a mini-tiled map of *Myh11-CreER^{T2}* integration locus was constructed.[68] To determine the copy number of *Myh11-CreER^{T2}*, qPCR was performed as above. Genomic DNA was diluted to 50 ng for input. Two primer sets targeting *ER^{T2}* of *Myh11-CreER^{T2}* were normalized to internal control primers (Supplementary Table 4). Real time quantitative PCR conditions were the following: step1 95°C for 3 min; step 2 95°C for 30 sec, 60°C for 30 sec, 72°C for 30 sec for 40 cycles.

Statistical analysis

A Shapiro-Wilk test was performed to determine whether data were normally distributed. Paired or unpaired one- or two-tailed *t*-tests were used for comparisons between experimental and control conditions and one- or two-way ANOVA with Tukey's posthoc testing for individual comparisons was done for multiple group comparisons. All data analyses were performed in GraphPad Prism 9 (GraphPad Software). Results are expressed as mean ± standard deviation. Probability values of $p<0.05$ were considered statistically significant.

Extended Data

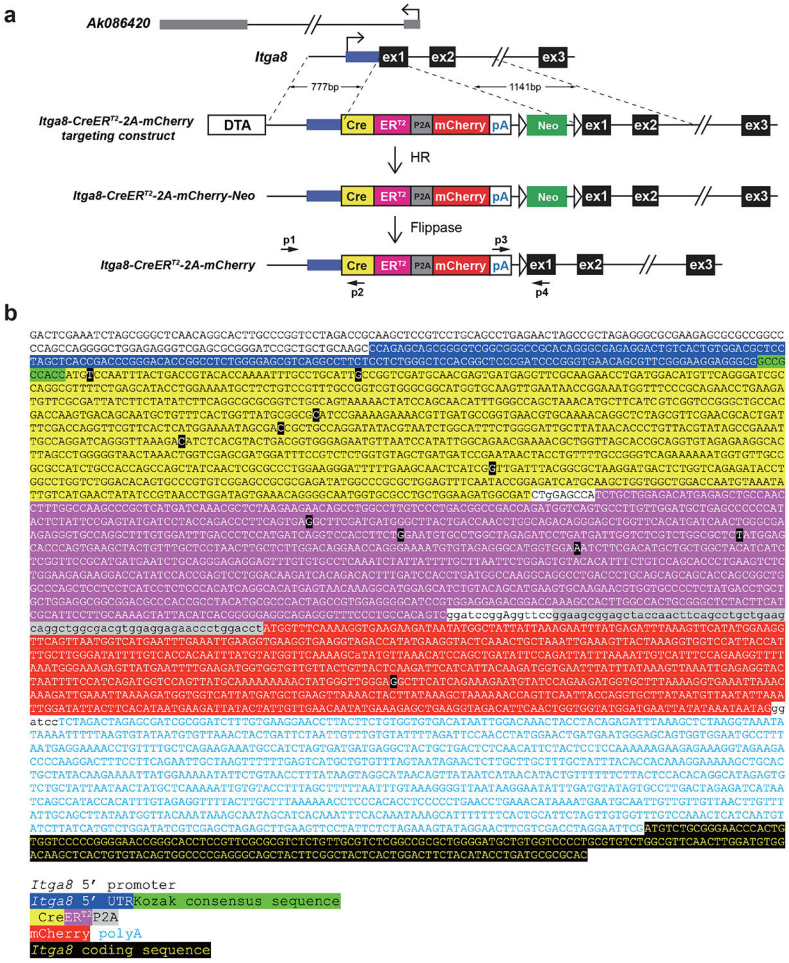

Extended Data Fig. 1. Strategy and sequence validation of *Itga8-CreER^{T2}*.

a, Partial *Itga8* locus, overlapping long noncoding RNA, and general strategy for mouse ESC targeting. The 22 amino acid P2A self-cleaving cassette (GSGATNFSLLKQAGDVEENPGP) allows for concurrent detection of the *CreER^{T2}* fusion and the mCherry reporter; however, mCherry fluorescence was not easily detected and therefore not pursued in this study. Small horizontal arrows (p1-p4) denote primers for PCR genotyping of mice. **b**, Nucleotide sequence of targeted knock-in cassette following Flippase-mediated removal of the *Neo* gene. Colors correspond to the schematic in **a**. Bases highlighted in black boxes represent codon-optimized substitutions from original sequences. HR, homologous recombination.

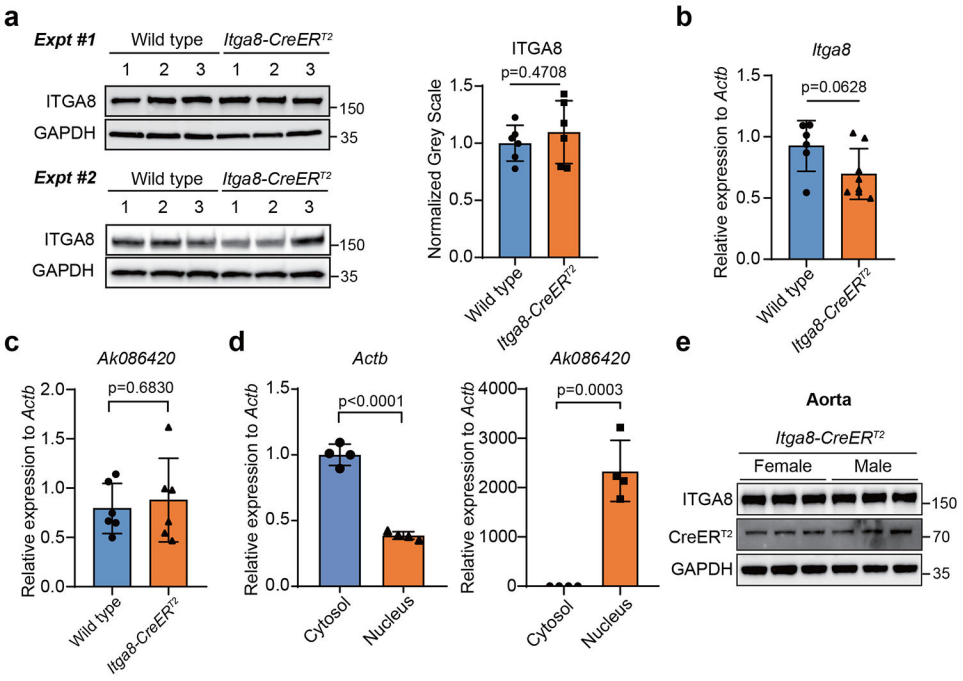

Extended Data Fig. 2. ITGA8 protein expression in heterozygous *Itga8-CreER^{T2}* mice.

a, Western blots of ITGA8 protein in two independent experiments performed by two independent investigators with quantitative data at right. n=6 independent male aortas for each condition. **b**, qRT-PCR analysis of *Itga8* mRNA and **c**, the antisense *Ak086420* long noncoding RNA in wild type versus *Itga8-CreER^{T2}* heterozygous aorta. n=6 male aortas per genotype. **d**, qRT-PCR of cytosolic versus nuclear *Ak086420* expression in wild type aorta (n=4 male aortas). Error bars represent the mean ± standard deviation; p-values determined by two-tailed, unpaired Student's t-test. **e**, Western blot of ITGA8 and CreER^{T2} in aorta of seven week-old male and female *Itga8-CreER^{T2}* heterozygous mice (n=3 independent mice of each sex). Molecular weight markers at right here and below are in kilodaltons.

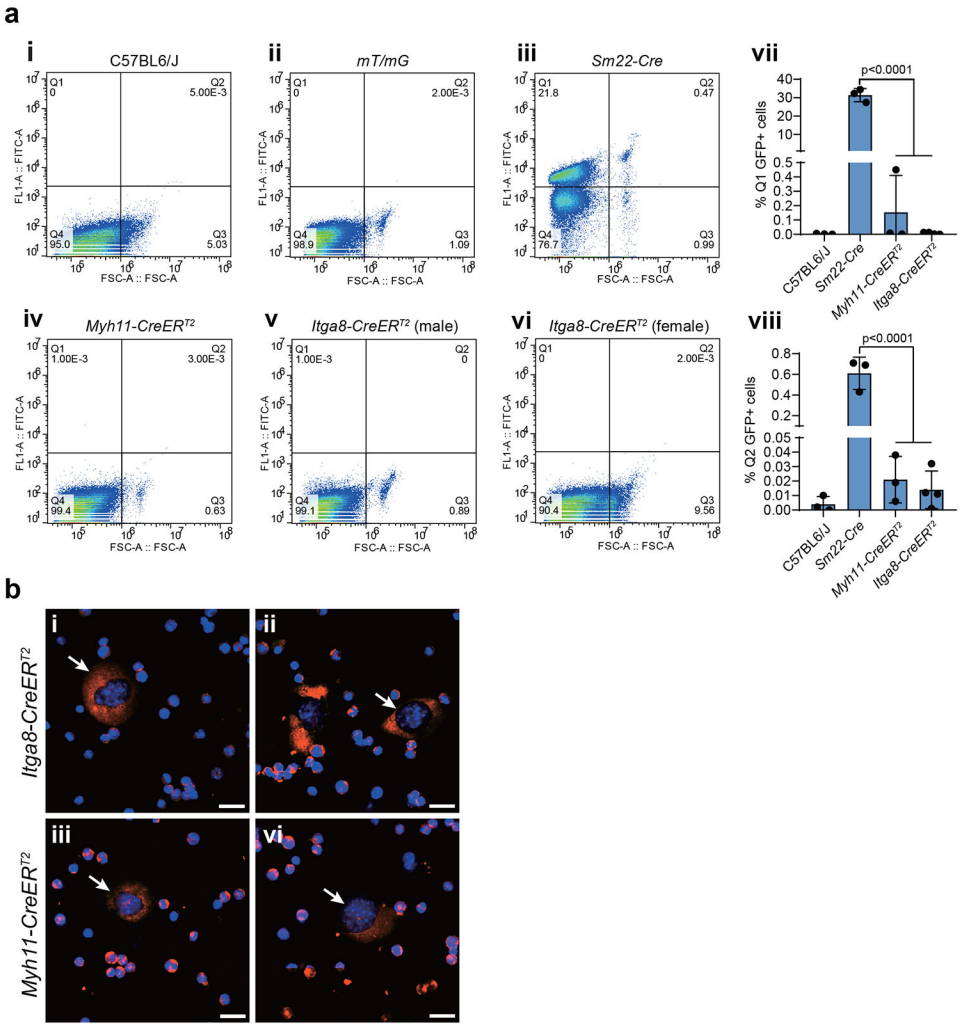

Extended Data Fig. 3. Recombination activity of different SMC *Cre* mice in myeloid cells.

a, Representative flow cytometry of GFP labeled cells from wild type C57BL/6J mice (**i**); *mT/mG* reporter mice (**ii**); and *mT/mG* in *Sm22-Cre* (**iii**); tamoxifen-treated male *Myh11-CreER*^{T2} (**iv**); tamoxifen-treated male *Itga8-CreER*^{T2} (**v**); tamoxifen-treated female *Itga8-CreER*^{T2} (**vi**) mice. Quantitative data for GFP+ circulating cells in upper left quadrant Q1 (**vii**) and upper right quadrant Q2 (**viii**) are shown for each *Cre* driver line (n=3 male mice per *Cre* line, save the *Itga8CreER*^{T2} line which represent male, n=2, and female, n=2, samples pooled for the graphs shown). The horizontal axis was set to the same threshold for all panels according to the apparent two populations of cells in the positive control (*Sm22-Cre-mT/mG*). The vertical axis divides two apparent populations of different sized cells in the *Sm22-Cre-mT/mG* strain. Note, as we did not gate for any surface markers in this study, we cannot label any quadrant as to cell type. Source of cells was from circulation cleared of red blood cells. Error bars represent the mean ± standard deviation. One-way ANOVA and posthoc testing revealed indicated p-values. See Supplementary Figure 5 for more details. **b**, Bone marrow aspirates of 10-week-old male *Itga8-CreER*^{T2} (i, ii) and *Myh11-CreER*^{T2} (iii, iv) mice (n=2 mice/genotype) carrying *mT/mG* reporter and treated with tamoxifen. Arrows indicate multi-nucleated megakaryocytes. Scale bars are 20μm.

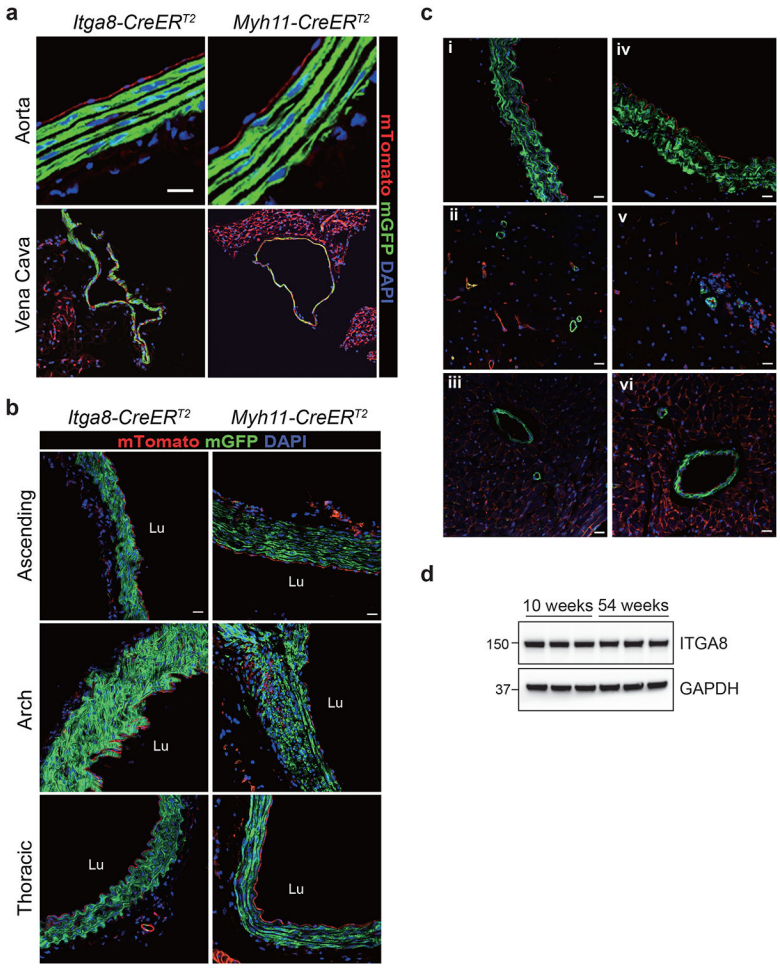

Extended Data Fig. 4. Comparative *Cre* activity in adult male and female blood vessels.

a, The GFP signal demonstrates recombination of the *mT/mG* reporter in medial SMCs of both the aorta and vena cava, whereas the red stained endothelium indicates the absence of recombination. Scale bar is 33μm for aorta and 100μm for vena cava. The aorta and vena cava of *Itga8-CreER^{T2}* was from a female mouse. **b**, Activity of each *CreER^{T2}* driver in indicated segments of male mouse aorta. Scale bars are 20μm for all panels. Lu, lumen of vessel wall. **c,** Tamoxifen-treated 54-week-old female (i-iii) and male (iv-vi) mouse thoracic aorta (i, iv), brain (ii, v), and heart (iii, vi). Each panel in **a** and **b** is representative of at least two independent male or female mice. Scale bars are all 20μm. **d,** Western blot of ITGA8 protein in 10-week-old versus 54-week-old female mouse aorta (n=3 independent mice per time point).

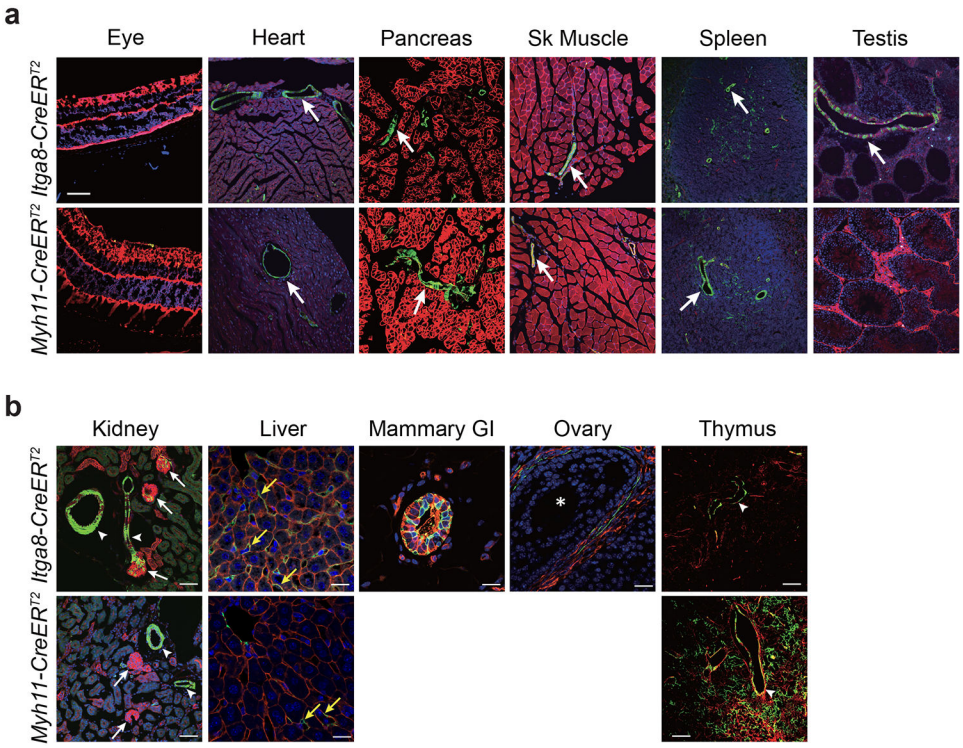

Extended Data Fig. 5. Comparative *Cre* activity in adult mouse tissues.

a, GFP signal restricted to VSMCs in blood vessels (arrows) of each indicated tissue type. **b**, GFP signal in VSMCs and non-VSMCs of indicated tissue types. White arrowheads, blood vessels of kidney and thymus; white arrows, glomeruli of kidney; yellow arrows, sinusoids of liver. *Itga8-CreER^{T2}*-mediated GFP signal was also present in myoepithelial cells of mammary gland and thecal cells around mature follicle (white asterisk) of ovary. All images were processed the same except for the Testis panel under *Itga8-CreER^{T2}*, which was uniformly enhanced to bring out more of the signal that otherwise would be too dark to visualize. Scale bar in **a** is 100μm for all images; scale bars in **b** are 50μm for kidney and thymus and 20μm for liver, mammary gland, and ovary. Data are representative of at least two independent male or female mice analyzed over the course of five years in two independent labs.

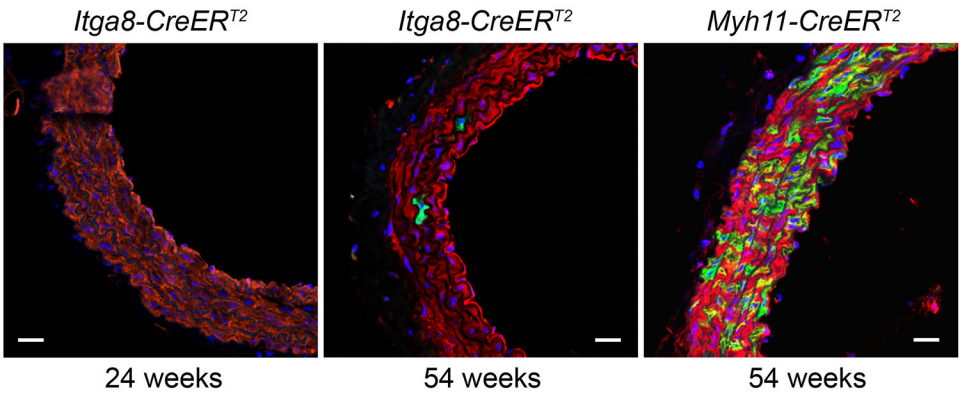

Extended Data Fig. 6. Leaky CreER^{T2} activity in aged mice.

Sections of aorta from 24-week-old or 54-week-old male *Itga8-CreER^{T2}* and 54-week-old *Myh11-CreER^{T2}* mice. The brightness in the 54-week *Itga8-CreER^{T2}* image was uniformly enhanced to better appreciate the GFP signal. Scale bars are 20μm for all panels. Images are representative of two independent mice.

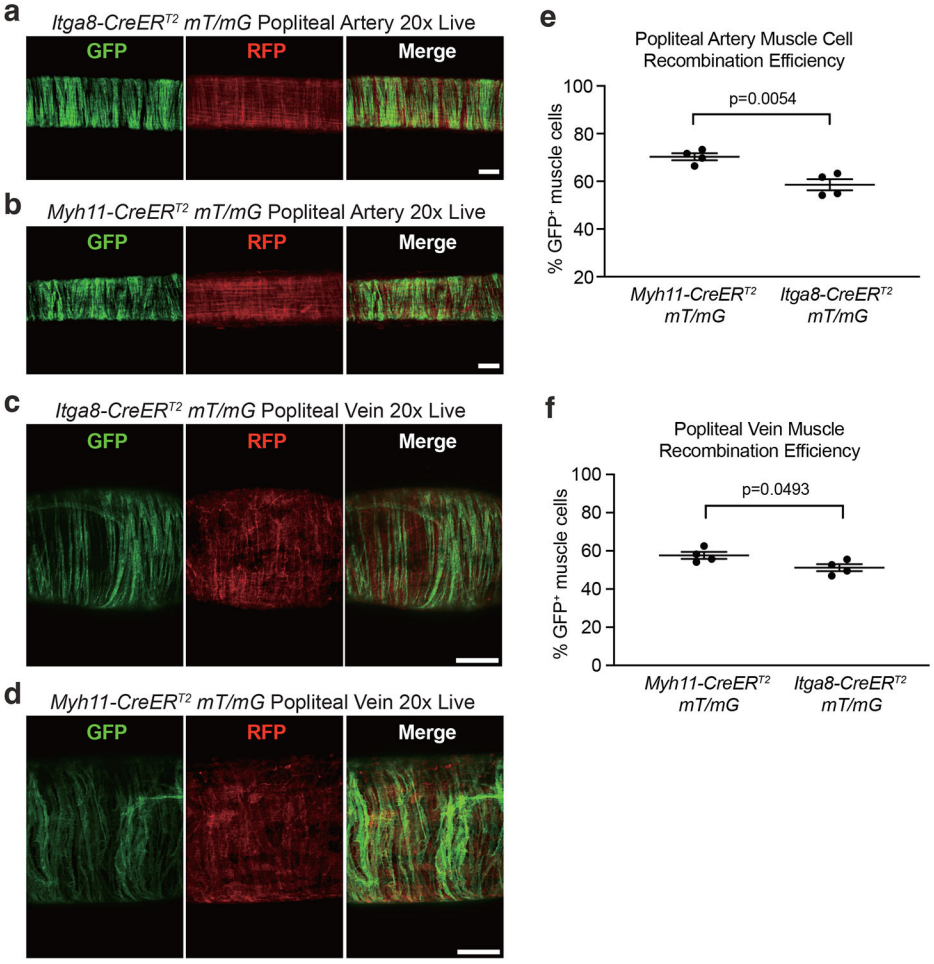

Extended Data Fig. 7. Quantitative activity of *Myh11-CreERT2* versus *Itga8-CreER^{T2}* in popliteal blood vessels.

Representative 2D maximum projections from confocal imaging of live GFP and tdTomato fluorescence popliteal artery (**a, b**) and vein (**c, d**) from *Myh11-CreER^{T2}* versus *Itga8-CreER^{T2}* with quantitation of each in panels **e** and **f**, respectively. n=4 male mice per genotype. Scale bars represent 50μm (**a, b**) and 100μm (**c, d**). Error bars in panels **e-f** represented by mean ± standard deviation; p-values determined by two-tailed, unpaired Student's t-test.

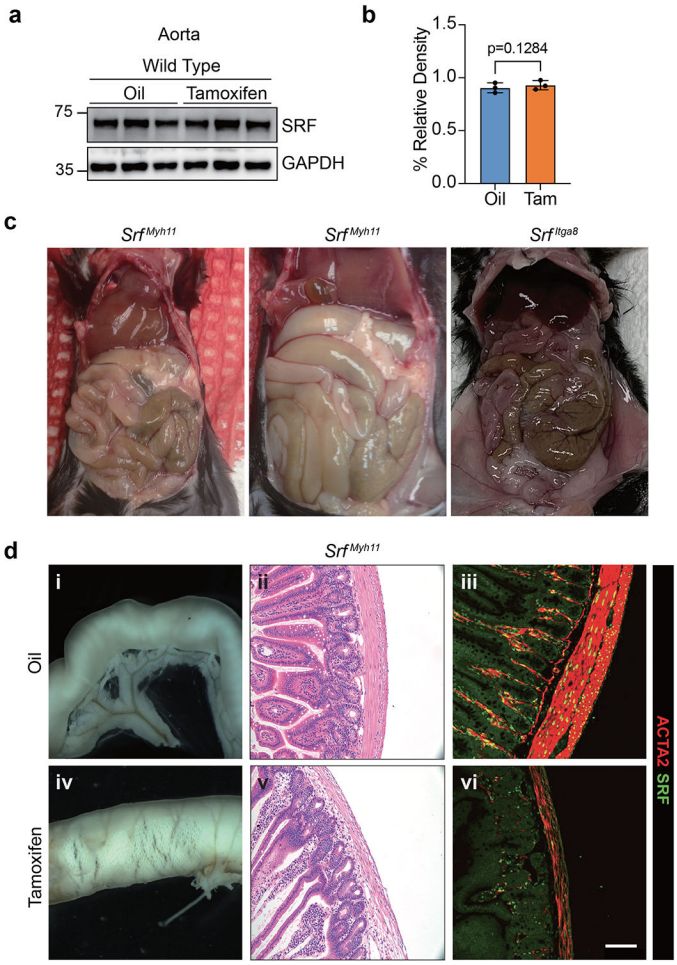

Extended Data Fig. 8. Intestinal phenotype in *Myh11-CreER^{T2}* versus *Itga8-CreER^{T2}* mediated knockout of serum response factor (*Srf*).

a, Western blot showing lack of effect of tamoxifen on SRF in wild type aorta (n=3 independent male mice per treatment). **b**, Quantitation of panel **a** represented by mean ± standard deviation; p-value determined by two-tailed, unpaired Student's t-test. **c**, Anatomy of abdominal cavity in the indicated *CreER^{T2}* driver mice used for *Srf* inactivation. The two *Srf^{Myh11}* images were from mice 14 days following tamoxifen administration, whereas the *Srf^{Itga8}* image was from a mouse 8 weeks after tamoxifen administration. **d**, Oil (panels i-iii) and Tamoxifen (panels iv-vi) treated *Srf^{Myh11}* mice with dissected gross intestine (i, iv), H&E stained intestine (ii, v), and immunostaining for SRF (green) and ACTA2 (red) in intestine (iii, vi). Scale bar is 100μm for ii, iii, v, and vi or 1mm for i and iv. Studies of panel **d** are representative of at least two independent male or female mice analyzed over the course of five years in two independent labs.

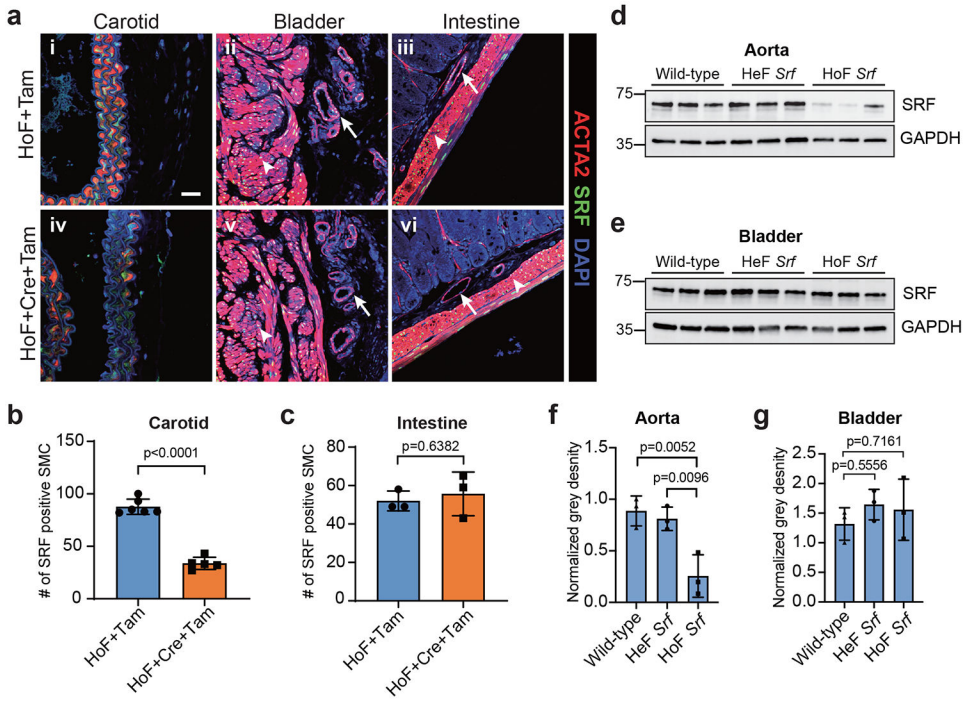

Extended Data Fig. 9. *Itga8-CreER*^{T2} mediated inactivation of *Srf* in adult mouse tissues.

a, Immunofluorescence confocal microscopy of sections of carotid artery (i, iv), bladder (ii, v), and intestine (iii, vi) from tamoxifen-treated male mice carrying homofloxed *Srf* alleles in the absence (i-iii) or presence (iv-vi) of *Itga8-CreER*^{T2} (abbreviated Cre). Sections were stained with antibodies to ACTA2 (red), SRF (green), and DAPI. Arrows and arrowheads point to blood vessels and visceral SMCs, respectively. Scale bar is 20μm for all panels. Data from each panel are representative of at least two independent mice. **b**, SRF positive VSMCs were counted in sections of carotid arteries from Tam-administered homozygous floxed *Srf* mice without *Cre* (HoF+Tam, n=6 male mice per condition) or homozygous floxed *Srf* mice with *Cre* (HoF+Cre+Tam, n=5 male mice per condition). **c**, Same quantitative measures as in panel **b** only from intestine (n=3 mice per condition). Western blots of SRF in aorta (**d**) and bladder (**e**) of indicated genotypes, all treated with the same schedule of tamoxifen. Corresponding quantitative data are shown for mouse aorta (**f**) and bladder (**g**) (n=3 mice per genotype). HeF, heterozygous floxed *Srf*; HoF, homozygous floxed *Srf*. Error bars are mean ± standard deviation. Student unpaired, one-tailed *t*-test was applied in **b** and **c**, and one-way ANOVA with Tukey's t-test for **f** and **g** to reveal indicated p-values in each graph.

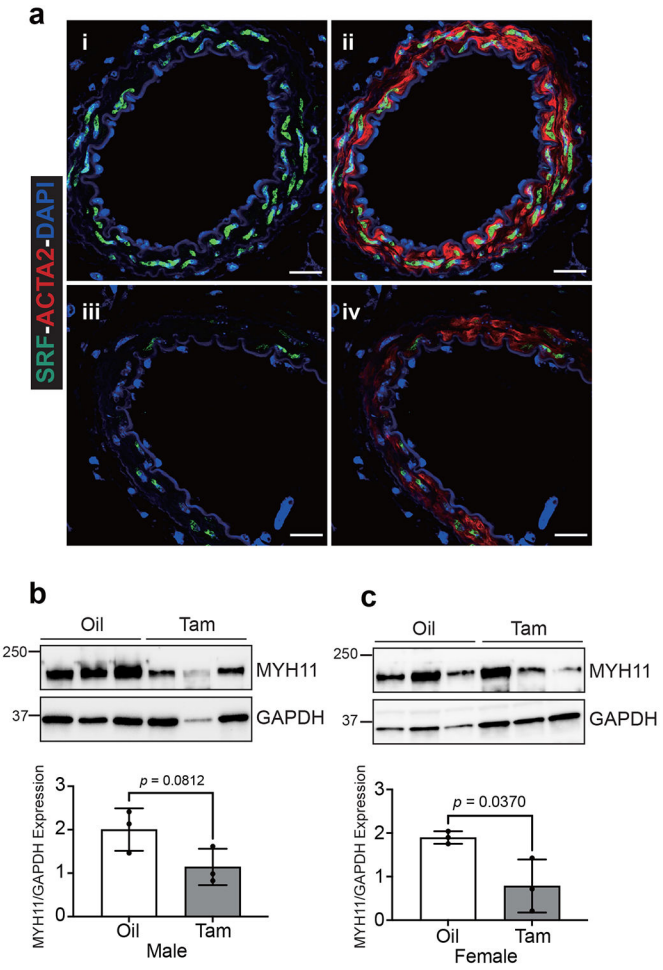

Extended Data Fig. 10. Contractile activity of mesenteric artery in *Srf*^{Itga8} conditional knockout mice.

a, Confocal immunofluorescence microscopy of SRF and DAPI alone (i, iii) and merged with ACTA2 (ii, iv) in mesenteric arteries of Oil control (i, ii) versus tamoxifen-treated (iii, iv) homozygous *Srf*^{Itga8} mice; scale bars are 20μm. Results shown are of two independent mice for each condition. Western blots of SRF target, MYH11, in Oil versus Tam-induced *Srf*^{Itga8} homozygous male (**b**) and female (**c**) mesenteric arteries. n=3 independent animals for each condition. Error bars represented by mean ± standard deviation; p-values determined by two-tailed, unpaired Student's t-test.

Supplementary Material

Refer to Web version on PubMed Central for supplementary material.

Acknowledgments

We thank members of the University of Rochester Medical Center Genomics Research Core for carrying out the RNA-seq experiments and generating Fig. 2e and the Electron Microscopy and Histology Core at Augusta University for performing the immunogold studies and generating Fig. 1b.

Sources of Funding

This work was supported by the American Heart Association post-doctoral grants 17POST3360938 to QL and CDA858380 to JLF; and National Institutes of Health grants R00HL146948 to JFL; HL155265 to EBC; HL122578 to MJD; HL122686 and HL139794 to XL; HL138987, HL136224, and HL147476 to JMM; EY026614 to LG; and R00-HL143198 to SDZ.

Data availability

RNA-seq data are available through the Gene Expression Omnibus (GSE138824 and GSE199244). Long-read data (informative reads only) are available through the NCBI SRA database, which can be downloaded from www.ncbi.nlm.nih.gov/sra) under BioProject number PRJNA82551. Original source data are included in Supplementary materials. Updates to Supplementary Table 1 are available upon request.

References

1. Sauer B Inducible gene targeting in mice using the Cre/lox system. Methods 14, 381–392 (1998). [PubMed: 9608509]
2. Gu H, Marth JD, Orban PC, Mossmann H & Rajewsky K Deletion of a DNA polymerase beta gene segment in T cells using cell type-specific gene targeting. Science 265, 103–106 (1994). [PubMed: 8016642]
3. Feil R et al. Ligand-activated site-specific recombination in mice. Proc Natl Acad Sci U S A 93, 10887–10890 (1996). [PubMed: 8855277]
4. Majesky MW Developmental basis of vascular smooth muscle diversity. Arteriosclerosis, Thrombosis and Vascular Biology 27, 1248–1258 (2007). [PubMed: 17379839]
5. Tasian G, Cunha G & Baskin L Smooth muscle differentiation and patterning in the urinary bladder. Differentiation 80, 106–117 (2010). [PubMed: 20541860]
6. Somlyo AP & Somlyo AV Signal transduction and regulation in smooth muscle. Nature 372, 231–236 (1994). [PubMed: 7969467]
7. Kuriyama H, Kitamura K, Itoh T & Inoue R Physiological features of visceral smooth muscle cells, with special reference to receptors and ion channels. Physiol Rev 78, 811–920 (1998). [PubMed: 9674696]
8. Owens GK, Kumar MS & Wamhoff BR Molecular regulation of vascular smooth muscle cell differentiation in development and disease. Physiological Reviews 84, 767–801 (2004). [PubMed: 15269336]
9. Chakraborty R et al. Promoters to study vascular smooth muscle: mistaken identity? Arteriosclerosis, Thrombosis and Vascular Biology 39, 603–612 (2019). [PubMed: 30727757]
10. Angstenberger M et al. Severe intestinal obstruction on induced smooth muscle-specific ablation of the transcription factor SRF in adult mice. Gastroenterology 133, 1948–1959 (2007). [PubMed: 18054566]
11. Mericskay M et al. Inducible mouse model of chronic intestinal pseudo-obstruction by smooth muscle-specific inactivation of the SRF gene. Gastroenterology 133, 1960–1970 (2007). [PubMed: 18054567]
12. He WQ et al. Myosin light chain kinase is central to smooth muscle contraction and required for gastrointestinal motility in mice. Gastroenterology 135, 610–620 (2008). [PubMed: 18586037]
13. Albinsson S et al. Smooth muscle miRNAs are critical for post-natal regulation of blood pressure and vascular function. PLoS One 6, e18869 (2011). [PubMed: 21526127]
14. Huang J et al. Myocardin is required for maintenance of vascular and visceral smooth muscle homeostasis during postnatal development. Proceedings of the National Academy of Sciences USA 112, 4447–4452 (2015).
15. Morano I et al. Smooth-muscle contraction without smooth-muscle myosin. Nature Cell Biology 2, 371–375 (2000). [PubMed: 10854329]

16. Niessen P et al. Smoothelin-a is essential for functional intestinal smooth muscle contractility in mice. Gastroenterology 129, 1592–1601 (2005). [PubMed: 16285958]
17. Halim D et al. Loss of LMOD1 impairs smooth muscle cytocontractility and causes megacystis microcolon intestinal hypoperistalsis syndrome in humans and mice. Proceedings of the National Academy of Sciences USA 114, E2739–E2747 (2017).
18. Li S, Wang DZ, Richardson JA & Olson EN The serum response factor coactivator myocardin is required for vascular smooth muscle development. Proceedings of the National Academy of Sciences of the United States of America 100, 9366–9370 (2003). [PubMed: 12867591]
19. Guzzardo PM et al. A small cassette enables conditional gene inactivation by CRISPR/Cas9. Sci Rep 7, 16770 (2017). [PubMed: 29196747]
20. Horii T et al. Efficient generation of conditional knockout mice via sequential introduction of lox sites. Sci Rep 7, 7891 (2017). [PubMed: 28801621]
21. Anzalone AV et al. Search-and-replace genome editing without double-strand breaks or donor DNA. Nature 576, 149–157 (2019). [PubMed: 31634902]
22. Gurumurthy CB et al. Reproducibility of CRISPR-Cas9 methods for generation of conditional mouse alleles: a multi-center evaluation. Genome Biol 20, 171 (2019). [PubMed: 31446895]
23. Bossy B, Bossy-Wetzel E & Reichardt LF Characterization of the integrin a8 subunit: a new integrin b1-associated subunit, which is prominently expressed on axons and on cells in contact with basal laminae in chick embryos. EMBO Journal 10, 2375–2385 (1991). [PubMed: 1714374]
24. Schnapp LM, Breuss JM, Ramos DM, Sheppard D & Pytela R Sequence and tissue distribution of the human integrin a8 subunit: a b1-associated a subunit expressed in smooth muscle cells. Journal of Cell Science 108, 537–544 (1995). [PubMed: 7768999]
25. Hartner A, Schocklmann H, Prols F, Muller U & Sterzel RB Alpha8 integrin in glomerular mesangial cells and in experimental glomerulonephritis. Kidney International 56, 1468–1480 (1999). [PubMed: 10504498]
26. Chen J, Maltby KM & Miano JM A novel retinoid-response gene set in vascular smooth muscle cells. Biochem Biophys Res Commun 281, 475–482 (2001). [PubMed: 11181072]
27. Zargham R & Thibault G a8b1 integrin expression in the rat carotid artery: involvement in smooth muscle cell migration and neointima formation. Cardiovascular Research 65, 813–822 (2005). [PubMed: 15721861]
28. Zargham R, Touyz RM & Thibault G a8 integrin overexpression in de-differentiated vascular smooth muscle cells attenuates migratory activity and restores the characteristics of the differentiated phenotype. Atherosclerosis 195, 303–312 (2007). [PubMed: 17275006]
29. Kitchen CM, Cowan SL, Long X & Miano JM Expression and promoter analysis of a highly restricted integrin alpha gene in vascular smooth muscle. Gene 513, 82–89 (2013). [PubMed: 23142384]
30. Muller U et al. Integrin a8b1 is critically important for epithelial-mesenchymal interactions during kidney morphogenesis. Cell 88, 603–613 (1997). [PubMed: 9054500]
31. Shen Z et al. Smooth muscle protein 22 alpha-Cre is expressed in myeloid cells in mice. Biochemical Biophysical Research Communications 422, 639–642 (2012). [PubMed: 22609406]
32. Wirth A et al. G12-G13-LARG-mediated signaling in vascular smooth muscle is required for salt-induced hypertension. Nature Medicine 14, 64–68 (2008).
33. Miano JM et al. Restricted inactivation of serum response factor to the cardiovascular system. Proceedings of the National Academy of Sciences USA 101, 17132–17137 (2004).
34. Alvarez-Aznar A et al. Tamoxifen-independent recombination of reporter genes limits lineage tracing and mosaic analysis using CreER(T2) lines. Transgenic Res 29, 53–68 (2020). [PubMed: 31641921]
35. Vanlandewijck M et al. A molecular atlas of cell types and zonation in the brain vasculature. Nature (2018).
36. Shimshek DR et al. Codon-improved Cre recombinase (iCre) expression in the mouse. Genesis 32, 19–26 (2002). [PubMed: 11835670]
37. Nicholls PK, Bellott DW, Cho TJ, Pyntikova T & Page DC Locating and characterizing a transgene integration site by nanopore sequencing. G3 (Bethesda) 9, 1481–1486 (2019). [PubMed: 30837263]

38. Xue B, Pamidimukkala J & Hay M Sex differences in the development of angiotensin II-induced hypertension in conscious mice. Am J Physiol Heart Circ Physiol 288, H2177–2184 (2005). [PubMed: 15626687]
39. Park C et al. Loss of serum response factor induces microRNA-mediated apoptosis in intestinal smooth muscle cells. Cell Death Dis 6, e2011 (2015). [PubMed: 26633717]
40. Retailleau K et al. Selective involvement of serum response factor in pressure-induced myogenic tone in resistance arteries. Arteriosclerosis, Thrombosis and Vascular Biology 33, 339–346 (2013). [PubMed: 23264443]
41. Galmiche G et al. Inactivation of serum response factor contributes to decrease vascular muscular tone and arterial stiffness in mice. Circ Res 112, 1035–1045 (2013). [PubMed: 23426017]
42. Herring BP, Hoggatt AM, Gupta A & Wo JM Gastroparesis is associated with decreased FOXF1 and FOXF2 in humans, and loss of FOXF1 and FOXF2 results in gastroparesis in mice. Neurogastroenterol Motil 31, e13528 (2019). [PubMed: 30565344]
43. Rashbrook VS, Brash JT & Ruhrberg C Cre toxicity in mouse models of cardiovascular physiology and disease. Nature Cardiovascular Research (2022).
44. Matthaei KI Genetically manipulated mice: a powerful tool with unsuspected caveats. J Physiol 582, 481–488 (2007). [PubMed: 17495035]
45. Perry MN et al. Annotated expression and activity data for murine recombinase alleles and transgenes: the CrePortal resource. Mamm Genome 33, 55–65 (2022). [PubMed: 34482425]
46. Buelow B & Scharenberg AM Characterization of parameters required for effective use of tamoxifen-regulated recombination. PLoS One 3, e3264 (2008). [PubMed: 18810268]
47. Sandlesh P, Juang T, Safina A, Higgins MJ & Gurova KV Uncovering the fine print of the CreERT2-LoxP system while generating a conditional knockout mouse model of Ssrp1 gene. PLoS One 13, e0199785 (2018). [PubMed: 29953487]
48. Meinke G, Bohm A, Hauber J, Pisabarro MT & Buchholz F Cre recombinase and other tyrosine recombinases. Chemical Reviews 116, 12785–12820 (2016). [PubMed: 27163859]
49. Clayton JA Applying the new SABV (sex as a biological variable) policy to research and clinical care. Physiol Behav 187, 2–5 (2018). [PubMed: 28823546]
50. Liao M et al. An X-linked Myh11-CreER(T2) mouse line resulting from Y to X chromosome-translocation of the Cre allele. Genesis 55 (2017).
51. Morgan AP, Bell TA, Crowley JJ & Pardo-Manuel de Villena F Instability of the pseudoautosomal boundary in house mice. Genetics 212, 469–487 (2019). [PubMed: 31028113]
52. Goodwin LO et al. Large-scale discovery of mouse transgenic integration sites reveals frequent structural variation and insertional mutagenesis. Genome Res 29, 494–505 (2019). [PubMed: 30659012]
53. Zargham R, Pepin J & Thibault G a8b1 integrin is up-regulated in the neointima concomitant with late luminal loss after balloon injury. Cardiovascular Pathology 16 212–220 (2007). [PubMed: 17637429]
54. Fuchs H et al. Mouse phenotyping. Methods 53, 120–135 (2011). [PubMed: 20708688]
55. Nishimichi N et al. Induced hepatic stellate cell integrin, alpha8beta1, enhances cellular contractility and TGFbeta activity in liver fibrosis. J Pathol 253, 366–373 (2021). [PubMed: 33433924]
56. Corliss BA et al. Myh11 lineage corneal endothelial cells and ASCs populate corneal endothelium. Invest Ophthalmol Vis Sci 60, 5095–5103 (2019). [PubMed: 31826231]
57. Armulik A, Abramsson A & Betsholtz C Endothelial/pericyte interactions. Circ Res 97, 512–523 (2005). [PubMed: 16166562]
58. Hess DL et al. Perivascular cell-specific knockout of the stem cell pluripotency gene Oct4 inhibits angiogenesis. Nat Commun 10, 967 (2019). [PubMed: 30814500]
59. Orlich MM et al. Mural cell SRF controls pericyte migration, vessel patterning and blood flow. Circ Res 131, 308–327 (2022). [PubMed: 35862101]
60. Miano JM Serum response factor: toggling between disparate programs of gene expression. Journal of Molecular Cellular Cardiology 35, 577–593 (2003). [PubMed: 12788374]

61. George SH et al. Developmental and adult phenotyping directly from mutant embryonic stem cells. Proceedings of the National Academy of Sciences USA 104, 4455–4460 (2007).

62. Schindelin J et al. Fiji: an open-source platform for biological-image analysis. Nat Methods 9, 676–682 (2012). [PubMed: 22743772]

63. Preibisch S, Saalfeld S & Tomancak P Globally optimal stitching of tiled 3D microscopic image acquisitions. Bioinformatics 25, 1463–1465 (2009). [PubMed: 19346324]

64. Ho Sui SJ, Fulton DL, Arenillas DJ, Kwon AT & Wasserman WW oPOSSUM: integrated tools for analysis of regulatory motif over-representation. Nucleic Acids Research 35, W245–W252 (2007). [PubMed: 17576675]

65. Gao P et al. Prime editing in mice reveals the essentiality of a single base in driving tissue-specific gene expression. Genome Biol 22, 83 (2021). [PubMed: 33722289]

66. Faulkner JL et al. Lack of suppression of aldosterone production leads to salt-sensitive hypertension in female but not male Balb/C mice. Hypertension 72, 1397–1406 (2018). [PubMed: 30571230]

67. Wu J et al. Inflammation and mechanical stretch promote aortic stiffening in hypertension through activation of p38 mitogen-activated protein kinase. Circ Res 114, 616–625 (2014). [PubMed: 24347665]

68. Bryant WB et al. CRISPR-LRS for mapping transgenes in the mouse genome. bioRxiv, 2022.2001.2005.475144 (2022).

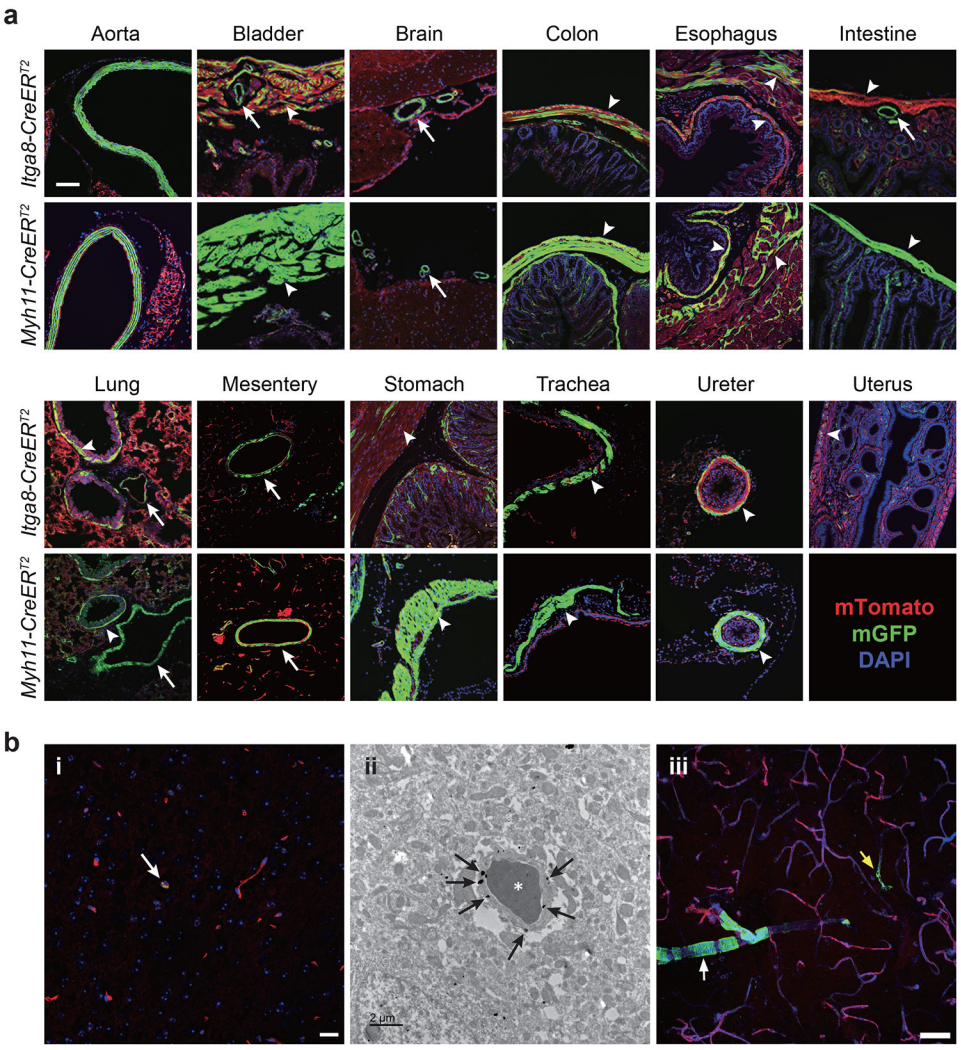

Fig. 1. Comparative recombination activity of *Itga8-CreER^{T2}* versus *Myh11-CreER^{T2}* in adult tissues.

a, Paired tissues from 10-week-old mice carrying indicated *CreER^{T2}* and *mT/mG* reporter. Green fluorescent protein (GFP), reflecting CreER^{T2}-mediated excision of tdTomato cassette in the *mT/mG* reporter, is primarily confined to SMCs. DAPI indicates nuclear staining. White arrows indicate blood vessels; white arrowheads indicate visceral smooth muscle cells. Scale bar represents 100μm for aorta and uterus and 50μm for all other panels. **b**, Minimal *Itga8-CreER^{T2}* activity in pericytes of brain shown by *mT/mG*-derived GFP fluorescence (arrow in panel i), immunogold (arrows) electron microscopy (ii), and 2D maximum projection confocal microscopy (iii). An arteriole (white arrow) and capillary (yellow arrow) are highlighted in panel iii. Asterisk in panel ii denotes a red blood cell. Scale bars are 20μm, 2μm, and 50μm for panels i, ii, and iii, respectively. Data are representative of at least two independent male or female mice analyzed over the course of five years in two independent labs.

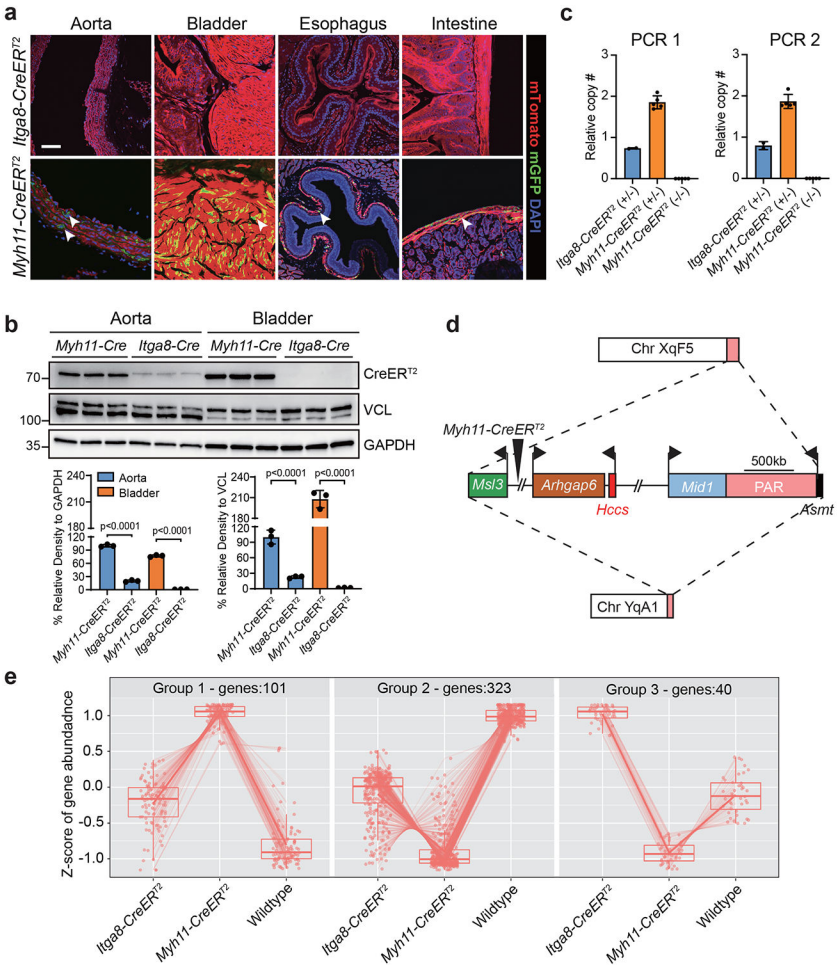

Fig. 2. Distinguishing features of the *Myh11-CreER^{T2}* mouse.

a, Tamoxifen-independent recombination activity in 10-week-old male *Myh11-CreER^{T2}* tissues. Arrowheads point to SMCs with leaky activity. Images of aorta and bladder replicated in two additional animals from two independent labs; images of esophagus and intestine replicated in one independent experiment. **b,** Western blot of CreER^{T2} protein from 8-week-old male mice from each *CreER^{T2}* driver (n=3 mice per genotype). Units of measure for molecular weight markers here and in all subsequent blots is in kilodaltons. p values determined by one-way ANOVA with Tukey's Student's t-test. **c,** qPCR of *Myh11-CreER^{T2}* transgene from adult spleen (n=5 wild type and *Myh11-CreER^{T2}* mice; n=2 *Itga8-CreER^{T2}* mice). Two primer pairs (PCR 1 and PCR 2) used that amplify non-overlapping sequences in *ER^{T2}*. **d,** Long read sequence mapping of approximate site-of-integration for *Myh11-CreER^{T2}* transgene (large triangle). Dashed lines represent initial translocation of the *Myh11-CreER^{T2}* transgene from X chromosome (top) carrying X-linked genes surrounding the *Myh11-CreER^{T2}* transgene (middle) to Y chromosome (bottom). Bent arrows indicate transcription start sites of each gene. Scale bar is an approximation. PAR, pseudoautosomal region. **e,** Bulk RNA-seq summary of differentially expressed genes in the absence of tamoxifen in 8-week-old male mice (n=3 mice per genotype). Group 1 represents significantly elevated genes in *Myh11-CreER^{T2}* aorta versus *Itga8-CreER^{T2}* and wild type;

Group 2 represents significantly elevated genes in wild type aorta; Group 3 represents significantly elevated genes in *Itga8-CreER*^{T2} aorta. A list of differentially expressed genes is provided in Supplementary Table 2. Values for box whisker plots can be found in the source data file.

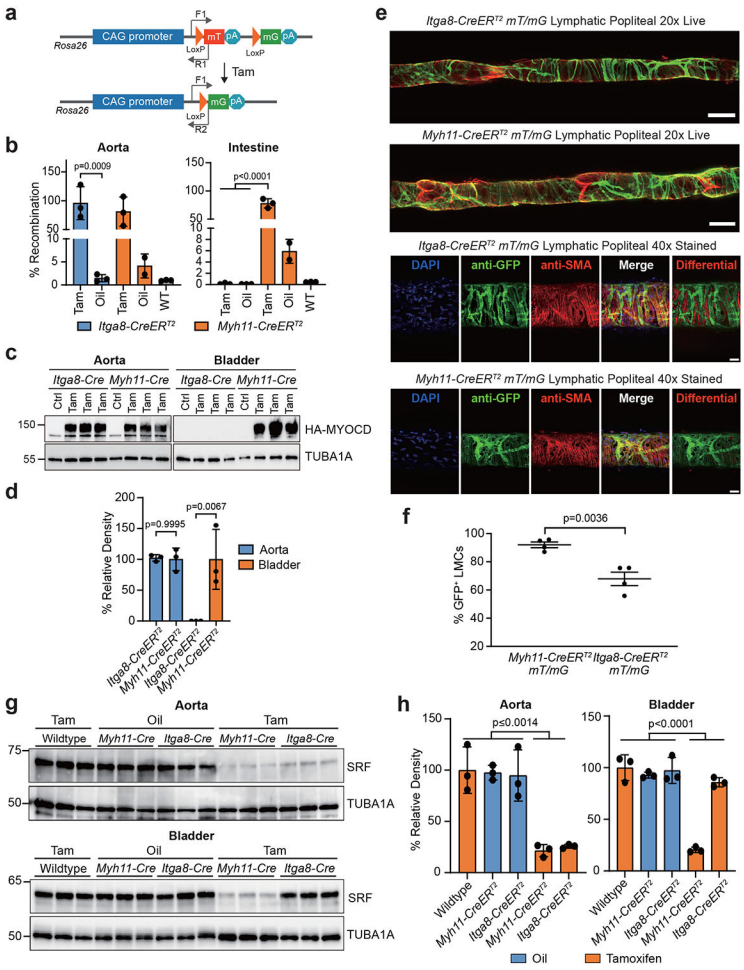

Fig. 3. Recombination efficiency of *Itga8-CreER^{T2}* versus *Myh11-CreER^{T2}*.

a, Schematic of *mT/mG* reporter at the *Rosa26* locus and position of primers (arrows) for measuring recombination. **b**, qPCR of genomic DNA following Oil or Tamoxifen (Tam) administration in each strain of *CreER^{T2}* (n=3 mice per condition and genotype, save Oil-treated *Myh11-CreER^{T2}* condition with n=2). Note leaky activity in Oil-treated *Myh11-CreER^{T2}*. **c**, Similar study design as in panel **b** only an inducible *Myocd* transgenic mouse was bred to each *CreER^{T2}* driver for Oil (Ctrl) or tamoxifen (Tam) administration and Western blotting for the presence of the HA-tagged MYOCD protein. **d**, Quantitative data of Western blots in panel **c**; (n=3 independent mice per genotype). **e**, Representative 2D maximum projections of popliteal lymphatic vessels isolated from each *CreER^{T2}* mouse (n=4 mice per genotype). Top panel, stitched maximum projections of live GFP and tdTomato fluorescence imaged with confocal microscopy at 20x. Note presence of GFP negative valves. Bottom panel, popliteal lymphatic vessels fixed and stained with DAPI, anti-GFP and anti-smooth muscle alpha actin (SMA) and imaged with confocal microscopy at 40x. The scale bars are 100μm for stitched images and 25μm for immunostained images. **f**, Quantitation of GFP+ fluorescence in lymphatic muscle cells (LMCs; n=4 mice per genotype). **g**, Western blot of SRF protein in aorta and bladders of each indicated genotype with Oil or Tam administration (n=3 mice per genotype). **h**, Quantitative data of panel

g; percent relative density to the TUBA1A loading control (n=3 independent mice per condition). Error bars represented by mean ± standard deviation. p values determined by one-way ANOVA and Tukey's t-test for panels **b** and **h** and unpaired two-tailed Student's t-test for panels **d** and **f**.

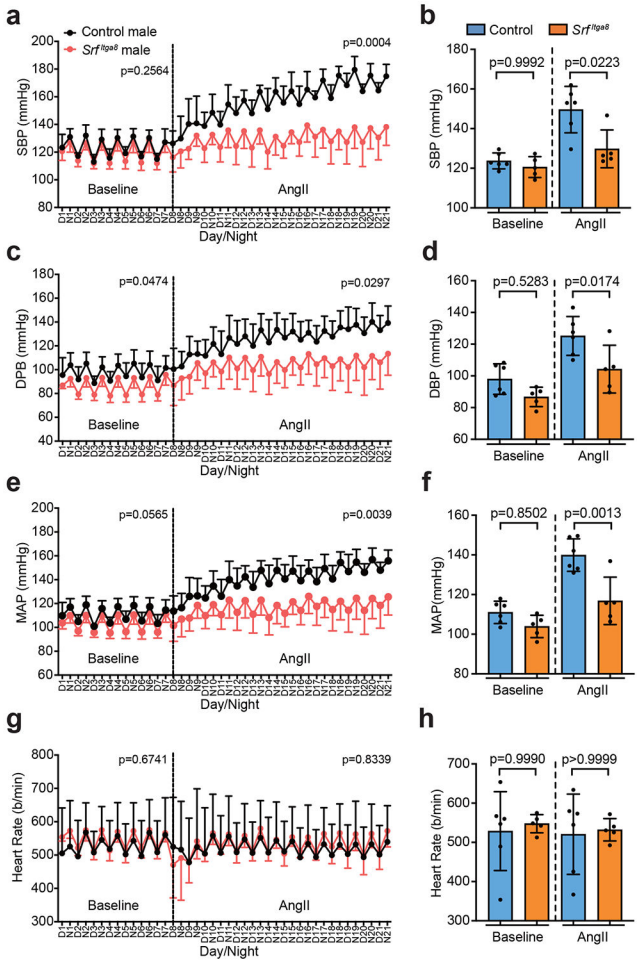

Fig. 4. Chronic blood pressure measurements in *Itga8-CreER^{T2}* mediated *Srf* knockout male mice.

Effects of *Srf* knockout (*Srf^{Itga8}*) on systolic blood pressure (**a, b**), diastolic blood pressure (**c, d**), mean arterial pressure (**e, f**) and heart rate (**g, h**) in male mice as measured by radio-telemetry over 3 weeks. Control mice here and in Figures 5 and 6 are oil-treated, homozygous floxed *Srf* mice carrying *Itga8-CreER^{T2}*. n=6 oil control and n=5 *Srf^{Itga8}* mice. Error bars represented by mean ± standard deviation. Each biological replicate represents the mean over days 1-7 (baseline) or days 8-21 (AngII). p values determined by two-way ANOVA for temporal study (**a,c,e,g**) and one-way ANOVA and Tukey's t-test for baseline and AngII (**b,d,f,h**).

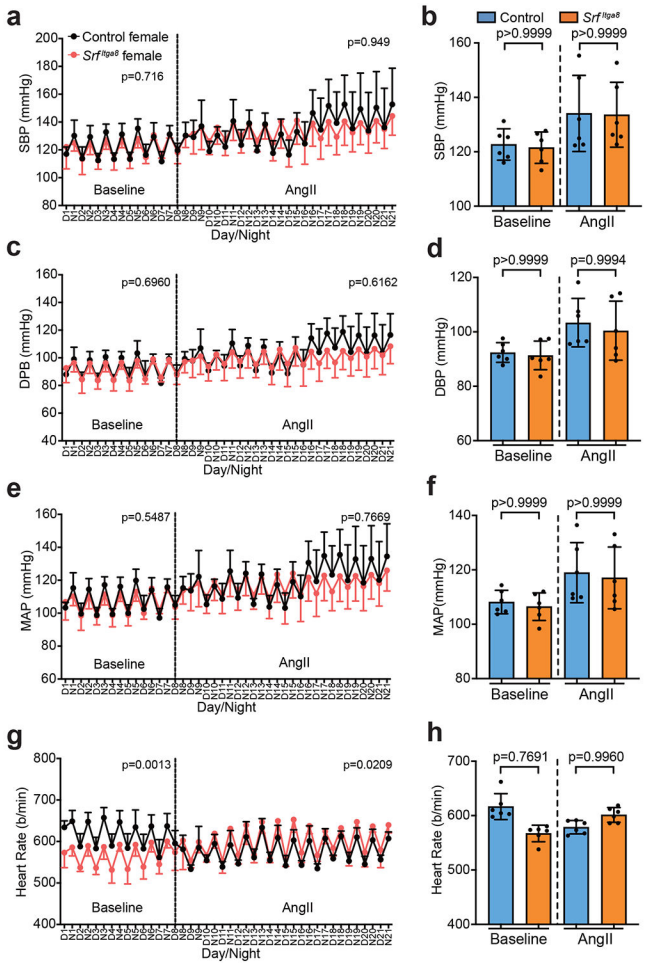

Fig. 5. Chronic blood pressure measurements in *Itga8-CreER^{T2}* mediated *Srf* knockout female mice.

Effects of *Srf^{Itga8}* on systolic blood pressure (**a, b**), diastolic blood pressure (**c, d**), mean arterial pressure (**e, f**) and heart rate (**g, h**) in female mice as measured by telemetry over 3 weeks. n=6 mice per condition. Error bars represented by mean ± standard deviation. Each biological replicate represents the mean over days 1-7 (baseline) or days 8-21 (AngII). p values determined by two-way ANOVA for temporal study (**a,c,e,g**) and one-way ANOVA and Tukey's t-test for baseline and AngII (**b,d,f,h**).

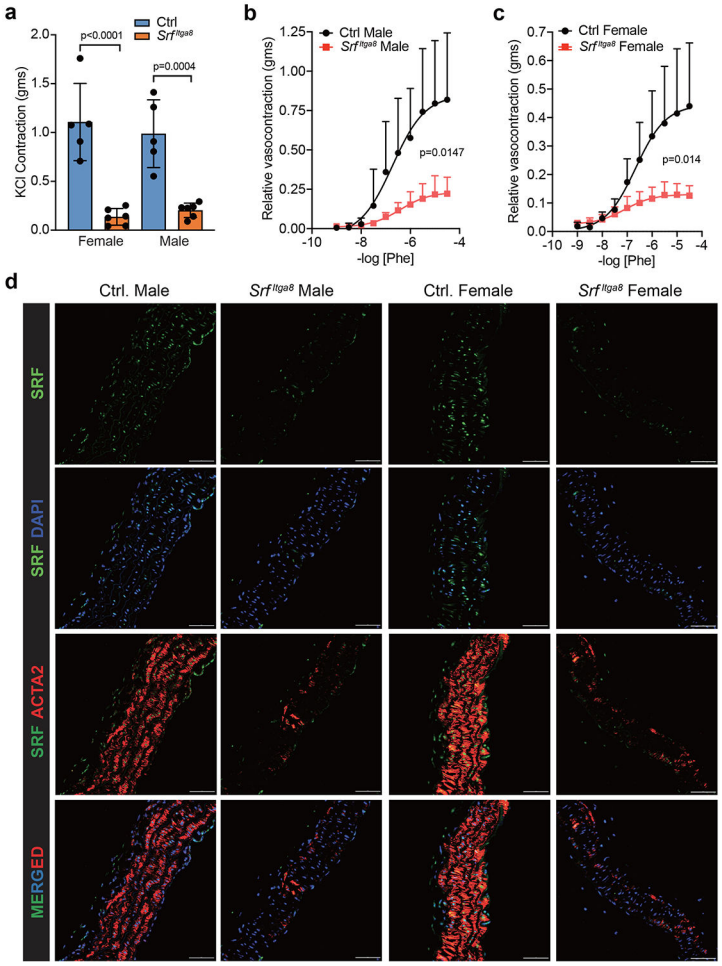

Fig. 6. Vascular contractile activity in *Itga8-CreER^{T2}* mediated *Srf* knockout mice.

a, KCl-stimulated contractile activity in female (n=5) and male (n=6) aorta under control or *Srf^{Itga8}* condition. The same groups of Male (**b**) and female (**c**) mouse aortas were treated with varying doses of Phenylephrine [Phe]. **d**, Confocal immunofluorescence microscopy of indicated proteins in control (Oil) and *Srf^{Itga8}* male and female aortic segments from the same mice used in KCl and Phe treatments. Images are representative of two independent mice. The scale bars are 50μm. Error bars represented by mean ± standard deviation. p values determined by one-way ANOVA and Tukey's t-test (**a**) or two-way ANOVA (**b,c**).

a

Gene	Heterozygous	Homozygous	log2FC	q value
Myh11	274,498	160,741	-0.743	1.39E-11
Cnn1	26,255	14,016	-0.858	2.65E-11
Csrp1	35,644	21,858	-0.683	2.65E-11
Flna	562,420	334,133	-0.721	3.06E-10
Tagln	93,661	52,342	-0.797	3.06E-10
Kcnmb1	3,803	2,289	-0.704	6.94E-10
Acta2	236,560	126,950	-0.845	7.60E-10
Mylk	55,146	35,710	-0.606	8.07E-09
Myl9	54,822	31,349	-0.759	6.29E-08
Actg2	4,715	2,451	-0.865	1.46E-07
Tspan2	7,220	4,063	-0.762	4.84E-06
Tgfb1i1	6,506	4,050	-0.635	8.11E-05
Lmod1	19,243	12,486	-0.581	3.43E-04
Actb	105,442	70,375	-0.542	1.30E-03
Srf	1,897	1,262	-0.539	3.73E-03

b

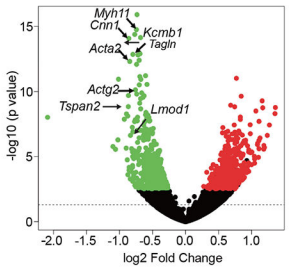

c

TF	JASPAR ID	Family	Z-score
SRF	MA0083.1	MADS	26.131
NR1H2-RXRA	MA0115.1	Hormone-nuclear Receptor	18.661
TLX1-NFIC	MA0119.1	Homeodomain-NFI-CCAAT-binding	16.998
MEF2A	MA0052.1	MADS	15.596
TBP	MA0108.2	TATA-binding	14.357
CEBPA	MA0102.2	Leucine Zipper	10.934
TEAD1	MA0090.1	Homeodomain	10.629
SPIB	MA0081.1	Ets	9.205
Hand1-Tcfe2a	MA0092.1	Helix-Loop-Helix	8.952
PPARG-RXRA	MA0065.2	Hormone-nuclear Receptor	8.787

d

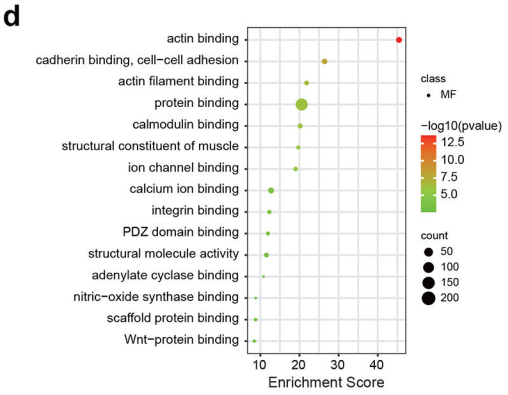

e

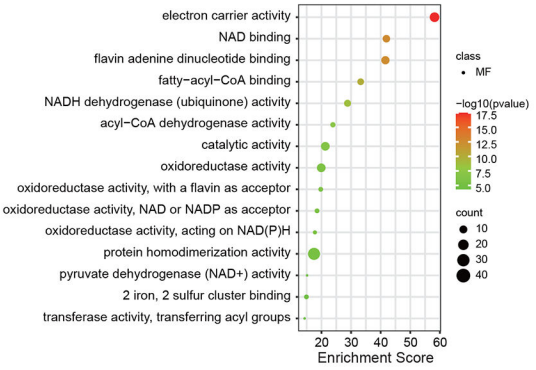

Fig. 7. Bulk RNA-seq of aortas from *Itga8-CreER^{T2}* mediated *Srf* knockout mice.

a, Down-regulated expression of SMC genes in aorta of heterozygous (n=2) versus homozygous (n=3) *Srf$^{\Delta tga8}$* knockout mice. **b**, Volcano plot of differentially expressed genes in *Srf$^{\Delta tga8}$* knockout aorta. **c**, oPOSSUM 3.0 analysis of over-represented transcription factor binding sites in promoter/intron of top 250 down-regulated genes in *Srf$^{\Delta tga8}$* knockout aorta. Enrichment scores for gene ontology terms (Molecular Function) related to downregulated (**d**) or upregulated (**e**) genes in *Srf$^{\Delta tga8}$* knockout aorta.

Table 1.

Contrasting characteristics of two SMC *Cre* drivers

Itga8-CreER^{T2}	**Myh11-CreER^{T2}**
Single-copy knock-in on Chr 2	Two-copy transgene on Chr Y
Chromosome stability	Exhibits t(Y;X) in ~ 3% of pups
Male and female studies	Male studies only
Lightly codon-optimized *Cre*	Heavily codon-optimized *Cre*
Low-level CreER^{T2} expression	High-level CreER^{T2} expression
More stable transcriptome	Altered transcriptome
Low-level leaky Cre in old mice	High-level leaky Cre in mice
Active preferentially in VSMCs	Equally active in all SMC lineages
Evades visceral myopathies	Causes many visceral myopathies
Active in mesangial, stellate, thecal, and myoepithelial cells of kidney, liver, ovary, and mammary gland, respectively	Active in corneal endothelial cells,[56] interstitial cells of the thymus, and in some stellate cells of liver
Low-level pericyte activity	Active in some pericytes[58]